UNIVERSITY OF NOVA GORICA
GRADUATE SCHOOL

# FUSION OF PLATINUM WIRE INTO THE CERAMIC BODY OF IMPLANTABLE STIMULATOR

MASTER'S THESIS

Miro ZDOVC

Mentor: Ph.D. Janez Rozman

Nova Gorica, 2011

UNIVERZA V NOVI GORICI
FAKULTETA ZA PODIPLOMSKI ŠTUDIJ

# ZATALITEV PLATINASTE ŽICE V KERAMIČNO OHIŠJE IMPLANTABILNEGA STIMULATORJA

MAGISTRSKO DELO

Miro ZDOVC

Mentor: Dr. Janez Rozman

Nova Gorica, 2011

First, I would like to thank my mentor dr. Janez Rozman to give me opportunity to work on very interesting field of biomaterials and implanting technology.
My work would not be the same if following people would not helped me regarding advices, editing, using equipment and performing analyses: Petra Juvan, Mojca Trauner (Emo Frite, Celje), dr. Sandra Gardonio, dr. Mattia Fanetti (Laboratorio Nazionale TASC), Mojca Vrčon, prof. dr. Matjaž Valant (UNG), mag. C.S. Praveen and dr. Michael W. Pitcher.
I would like to thank members of committee: prof. dr. Boštjan Žekš, prof. dr. Igor Mekjavič and especially prof. dr. Manfred Bijak for reviewing and commenting of the manuscript so that presented work is having a proper form.

*Moje delo je posvečeno moji mladi družini – Lari, Mihcu in Tanji.*

*Moji Mami, ki ima največje, najmehkejše in najtoplejše srce na svetu.*

FUSION OF PLATINUM WIRE INTO THE CERAMIC BODY OF IMPLANTABLE STIMULATOR

Abstract

The purpose of this work was to develop an appropriate method for manufacturing a hermetically sealed feedthrough for medical implants. Presented work was a pilot study with pre-selected materials (Macor ceramic for housing and Pt for wires). We used frits as bonding material of ceramic with metal. With different analyses we tried to proof if the introduced methodology provided an adequate seal for manufacture the second generation of the implanted unit.

Material selection and design, which was the initial part of the project, were based on the first generation of implanted gait correctors made by ITIS, d.o.o, Center for Implantable Technology and Sensors, Ljubljana, Slovenia. Three devices of the first generation were implanted in the patients.

Feedthroughs were formed by the fusion of Pt wire with Macor ceramic, using molten frits at temperatures up to 1000 ° C in an oxidative atmosphere.

For pilot study we made one sample for each frit/series combination.

When joining ceramic and metal in hermetically sealed feedthroughs six different frits were used with a composition in part similar to that of Macor ceramic.

All work was performed in compliance with good laboratory practice (GLP) regulations; particularly in respect to a clean environment and data storage during manufacturing.

Four series of feedthroughs were made. The first series were sealed at a temperature of 900 °C and the second at 1000 °C. Within this first series, the surfaces of the feedthroughs were coated with Pt (outer side of crucible) and Ti (inner side) using two different PVD (physical vapor deposition) technologies. The sealing cycle at 1000 °C was repeated 3 times. The third and fourth series were sealed at 1000 °C using fine machine ground frits to test the influence of particle size on porosity formation.

To obtain information about the quality of incoming materials and manufactured feedthroughs, several analyses were performed including TAPP (thermochemical calculation software for prediction of microstructure constituents) and XRD of Macor and frits, followed by examination of the feedthroughs (optical microscopy and SEM/EDX analyses).

Best results were obtained using frit R4 followed by frits R5 and R6 at sealing temperature of 1000 °C and with three steps of sealing (second series). The influence of milling is apparent; still, the porosity remains present in all formed feedthroughs. For that matter, it is necessary to include vacuum step. Formation of Macor/frit interphase was successful and wetting of the Pt wire was appropriate within feedthroughs R6-S1 and R6-S2. Achieved quality of the sealing along with selected technology and materials made successful first step for manufacturing the second generation of the feedthroughs for the implant unit.

Keywords

Gait corrector, implant, neuromuscular stimulator, Macor, frit, biomaterial, feedthrough, hermetic seal

ZATALITEV PLATINASTE ŽICE V KERAMIČNO OHIŠJE IMPLANTABILNEGA STIMULATORJA

Povzetek

Namen tega dela je bil razvoj metodologije za izdelavo hermetično zaprtega skoznika za medicinske implantate. Kot osnova za izbiro materialov in oblikovanje implantabilnega dela je služila uspešna implantacija prve generacije nevromuskulatornega stimulatorja za korekcijo hoje podjetja ITIS, d.o.o. Implantibilna tehnologija in senzorji, Ljubljana, Slovenija.

Razvoj hermetično zaprtega skoznika je del trenutne aktivne razvojne faze izdelave stimulatorja. Predstavljeno delo, pilotna izdelava druge generacije je potekala z zatalitvijo platinaste žice v keramično ohišje (Macor keramika) s staljeno frito pri temperaturah do 1000 °C v oksidativni (zračni) atmosferi. Za dosego hermetičnega spoja med kovino in keramiko smo uporabili 6 različnih frit s kemijsko sestavo podobno Macor keramiki, s čimer smo dosegli dobro zlivanje materialov. Za vsako kombinacijo frita/serija se je izdelal po eden vzorec.

Pri izdelavi skoznikov smo se držali načel dobre laboratorijske prakse (DLP), ki so vključevala načrtovanje in izvajanje del ter ustrezno dokumentiranje in arhiviranje rezultatov.

V okviru zastavljene naloge smo izdelali štiri serije skoznikov. Prva serija je vključevala taljenje frit na 900 °C. Dodatno smo na površino spojev nanesli kovine v tanki prevleki. Z uporabo različnih tehnologij je bila na zunanjo stran nanesena platina ter na notranjo stran titan. Naslednje serije vzorcev smo naredili pri temperaturi 1000 °C. Pri drugi seriji zataljevanja je bil postopek ponovljen trikrat, pri čemer smo vsakič dodali spoju dodatno količino frite. Medtem ko smo frite za prvi dve seriji pripravili ročno z drobljenjem v terilnici, smo naslednji dve seriji vzorcev pripravili v napravi za mletje, kjer je moč doseči zelo fino in izenačeno velikost delcev. Z različnim pristopom smo poskušali ugotoviti vpliv oblike in velikosti mletih frit na tvorjenje spoja na faznih mejah frita/ keramika (Macor) in frita/kovina (Pt).

V prvi fazi izdelave smo uporabili orodja, s katerimi smo določili osnovne lastnosti frit, kot so karakteristične temperature in razmerje med steklasto in kristalno fazo. Pri tem smo uporabili programsko opremo TAPP za določevanje termodinamskih lastnosti materialov ter rentgensko praškovno analizo.
Sklepna faza je bila uporaba optične mikroskopije s primerjavo kakovosti izdelanih skoznikov. Zaradi omejene možnosti povečave in analize z optično mikroskopijo smo dodatno analizirali dva izbrana skoznika z vrstičnim elektronskim mikroskopom in energijsko disperzivno rentgensko spektroskopijo (SEM/EDX).

Ključne besede
Implantabilen stimulator za korekcijo hoje, implantat, nevromuskularni stimulator, Macor, frita, biomaterial, skoznik, hermetični spoj

ZATALITEV PLATINASTE ŽICE V KERAMIČNO OHIŠJE IMPLANTABILNEGA STIMULATORJA

## Uvod

V 21. stoletju je zdravje še vedno eden izmed najpomembnejših dejavnikov v našem življenju, česar pa se običajno zavemo šele ob njegovi izgubi. Z dobro razvito mrežo zdravstvenega varstva se nam dandanes ob izgubi zdravja, invalidnosti ali fizično neestetske podobe ni potrebno boriti za preživetje. Kot simbol današnje materialistične podobe pa nas lahko okolica kaj hitro umesti v marginalizirano družbeno skupino ljudi, s čimer smo potisnjeni na rob socializiranosti.

Mogoče ravno zato doživlja plastična, rekonstruktivna in estetska kirurgija izreden razvoj. Pozitivna stran razvoja zajema številna področja, vključujoč tudi razvoj biomaterialov. Čeprav je pri teh poudarek predvsem na implantatih, pa se počasi, a vztrajno povečuje tudi uporabnost na zunaj telesnih sistemih. Ocenjeno je, da ima vsak 17. človek razvitega sveta eno vrsto implantata, vodilne so seveda ZDA. Celotna industrija na področju biomaterialov ima okoli 100 milijard $ letnega prihodka.

Eden izmed implantatov je nevromuskulatorni stimulator za korekcijo hoje [1-4], ki se uporablja pri bolnikih s hemiplegijo, ko je prisoten tudi zmanjšan obseg gibljivosti in motena funkcija mišic v spodnjem delu noge. Za to bolezen je značilen asimetričen vzorec hoje. Najpomembnejši del stimulatorja je implantiran del, katerega najšibkejši člen predstavlja skoznik. Funkcija skoznika je povezovanje elektronike v ohišju in stimulacijskih elektrod preko žic. Izziv izdelave predstavlja spajanje različnih materialov kot n.pr. keramike in kovine. Poleg tega, da mora biti spoj hermetično nepropusten, mora zdržati tudi vse mehanske obremenitve, ki se pojavljajo tako zaradi kombinacije različnih materialov kot tudi zaradi gibanja implantata znotraj telesa.

Po nekaterih podatkih naj bi bilo v letu 2006 kar 75 % okvar implantatov, povezanih z vdorom tekočin v ohišje implantata, kar pomeni, da skoznik ni opravil svoje funkcije. Nedelovanje implantata ne pomeni samo nujne operacije in odstranitve le-

tega. V primeru, da spoj na skozniku prepušča telesne tekočine v ohišje, te povzročijo kratek stik na vgrajeni elektroniki in s tem nedelovanje. Če te tekočine preidejo nazaj v telo, lahko s seboj nosijo kovinske ione iz elektronskega vezja. Posledice se kažejo v hudih zastrupitvah. S tega stališča je proces izdelave ustreznega skoznika zelo kompleksno in odgovorno delo. Sistematično načrtovanje materialov in tehnologij je ključnega pomena ter kot tako dobra popotnica do kasnejšega uspeha.

Testiranje biomaterialov je razdeljeno na biokompatibilne teste, teste hermetičnosti, karakterizacijo materialov in mehanske teste, kamor spada tudi korozija. Za te teste so navedeni številni standardi (ISO, ASTM), je pa zanimivo, da znotraj teh posamezni testi niso določeni. Zgolj od proizvajalca biomaterialov oz. implantatov je odvisno, katere teste bo le-ta opravil in kako. Posledice na zelo občutljivem področju se kažejo celo pri velikih podjetjih, ko se ugotovi, da je povsem novo razvit implantat po prvih implantacijah v človeškem telesu označen kot nevaren in neprimeren.

## Materiali in biokompatibilnost

Na področju medicine se uporabljajo praktično vse skupine inženirskih materialov [5-7]: keramika, kovine, polimeri, kompoziti, stekla, karbon in naravni biomateriali. Kot biomaterial je vsestransko uporabna keramika (tabela 1) [8], ki je lahko po svoji funkciji bioinertna, biaktivna ali biorazgradljiva. Kovine (tabela 2) [8] se v glavnem uporabljajo kot bioinertni material zaradi dobrih mehanskih lastnosti, so pa problematične zaradi sproščanja ionov, ki lahko v telesu povzročijo neželene reakcije. Ravno zaradi tega se uporabljajo predvsem zlitine, kot elementi nastopajo plemenite kovine in titan. Razvoj polimernih materialov (tabela 3) [8] ima vodilno vlogo v sistemih zunaj živega organizma (ex-vivo).

Glede na namembnost ločujemo tri vrste biomaterialov: biorazgradljive, bioaktivne ter bioinertne. Tipičen primer biorazgradljivih so šivi, ki razpadejo med celjenjem rane. Bioaktivni materiali se uporabljajo najpogosteje pri celjenju zloma kosti, ko se

material aktivno veže s kostjo. Implantat kot je nevromuskulatorni stimulator pa mora biti bioinerten.

Lastnost biomaterialov je, da so biokompatibilni [11,13]. Po definiciji to pomeni, da med implantatom in telesom ne sme priti do reakcij, ki bi imele opazen učinek na tkiva in telesne tekočine (zagotoviti se mora ustrezen biološki odziv - biokompatibilnost) ali na mikrostrukturo in mehanske lastnosti implantata. Biološki odziv je zelo kompleksna zadeva in še vedno ni popolnoma razumljen. Najnovejši trendi na področju biomaterialov ne zagovarjajo več bioinertne površine implantata, temveč se razvija materiale s površinskimi sloji, ki omogočajo aktiven stik s plazmo in telesnimi tekočinami – le v tem primeru namreč lahko pričakujemo biokompatibilnost, sicer telo zazna tujek v tej meri, da ga zavrne.

## Nevromuskulatorni stimulator za korekcijo hoje

Nevromuskulatorni stimulator za korekcijo hoje [2, 3] se uporablja za rehabilitacijo hemiplegičnih bolnikov zaradi kapi, sladkorne bolezni ali poškodbe glave.

Stimulator je sestavljen je iz zunanje in notranje enote. Dela zunanje enote (slika 3) [3] sta zunanji stimulator in stikalo na peti čevlja, medtem ko implantiran del (slika 4) [3] sestavljajo ohišje, elektroda na ohišju in platinasta žica z elektrodo za stimulacijo živca.

### Princip delovanja

V zadnji stopnji desnega položaja koraka se leva peta dotakne tal. Z aktiviranjem stikala na peti čevlja se impulzi prenesejo na stimulacijsko elektrodo, ki v naslednji fazi - zgodnji fazi desnega zamaha prične s stimulacijo skupnega peronealnega živca (CPN) (sliki 22a, b). Selektivna stimulacija tega živca je namenjena oživitvi funkcije dveh mišic – prednje golenčne mišice (tibialis anterior - TA) in kratke mečne mišice (peroneus brevis – PB). Glavna funkcija prednje golenčne mišice je dorzalna fleksija v zgornjem skočnem sklepu (dvig stopala v gležnju) ter inverzija (zvin stopala navznoter) in addukcija v spodnjem skočnem sklepu; njena aktivnost je pomembna

v zgodnji fazi zamaha, ko stopalo dvignemo. Funkcija kratke mečne mišice je plantarna fleksija (spust stopala v gležnju) in everzija (zvin stopala navzven); aktivna je v pozni fazi zamaha do trenutka, ko se desna noga dotakne tal in gre gleženj v dorzifleksijo.

Namen stimulacije skupnega peronealnega živca je torej selektivna reaktivacija dveh mišic, kar pripomore k izboljšani simetriji vzorca hoje. Pri tem je pomembno, da delovanje ene mišice vpliva na preostale, ki tudi sicer sodelujejo v gibanju. Raziskave[1] so pokazale, da je selektivno in postopno aktiviranje vlaken skupnega peronealnega živca doseglo izboljšanje oživčenja zgoraj omenjenih mišic.

# Praktični del

## Izbira materialov

Pri prvi generaciji implantabilne enote se je izbira materialov izkazala za pravilno, razvoj je bil potreben le na izdelavi skoznika, kjer so se pokazale težave. S tem je bilo obdržano ohišje implantata iz Macor keramike in izbira platinastih žic kot prevodnikov impulzov. Pregled strokovne literature in dostopnost tehnologij, ki so nam bile na voljo v okviru naloge, je delno zožil izbor materialov. Idejna zasnova naloge je bila, da se poišče partnerje na ožjem geografskem območju, po možnosti iz Slovenije. Tako smo se povezali s proizvajalcem frit, podjetjem Emo Frite d.o.o. iz Celja.

## Ohišje in pokrov

Macor keramika [56-58] ima številne tehnološke lastnosti, ki omogočajo uporabo tega materiala na različnih področjih vključno z medicino in vesoljsko tehnologijo. Glede na klasično keramiko ima precej nizko zgornjo temperaturo trajne uporabe (800 °C), vendar pa je brez poroznosti. Njena pomembna odlika je možnost strojne obdelave z navadnimi orodji. Strošek izdelave je zato nižji od konkurenčnih, sam material pa je tudi cenovno primerljiv. Vzrok dobre obdelovalnosti je mikrostruktura

Macor keramike, ki jo sestavlja 55 % mica mikro kristalov v borosilikatni steklasti osnovi (slika 21).
Z drugimi materiali se lahko veže z uporabo različnih postopkov kot n.pr. s spajkanjem, taljenjem, sintranjem in uporabo mehanskih spojev. V sklopu naloge smo se odločili, da bi bilo najprimerneje uporabiti postopek zataljevanja v prisotnosti kisika.

**Stimulacijske elektrode in žice**

Platina se uporablja v medicini zaradi njene biokompatibilnosti. Kemijska stabilnost preko širokega električnega potenciala omogoča primernost uporabe za stimulativne elektrode. Raziskave podjetja ITIS d.o.o. [64-66] so biokompatibilnost potrdile, ko pri analizi implantabilnega dela ni bilo zaznanih reakcij med površino elektrod in obdajajočim tkivom.
Odpornost na oksidacijo in visoko tališče platine sta vzrok, da se uporablja v kombinaciji s steklom za zataljevanje v industriji in znanstveni opremi že od 19. stoletja.
Platina in frita ne tvorita medfaznega sloja ampak frita zgolj omoči površino platine. Skoznik je zato na tem delu mehansko najšibkejši, z izboljšano geometrijo pa je mogoče tudi ta spoj mehansko utrditi na podoben način, kot smo to naredili z oblikovanjem izvrtine skoznika.

**Frite**

Pri izbiri frit (tabela 8) smo želeli doseči kemijsko sestavo podobno Macor keramiki oziroma borosilikatni fazi. Z izbiro šestih frit smo poskušali določiti vpliv sestave in elementov znotraj nje na tvorjenje medfaznega sloja na fazni meji Macor/frita in omočenju Pt s frito. Zaradi omejitve pri dokaj nizki zgornji temperaturi uporabe Macor keramike smo predvidevali, da bo aktivno vlogo pri oblikovanju medfaznega sloja (do 1000 °C) imel le steklasti del mikrostrukture keramike in frite.

Za določevanje ustrezne sestave frit in pogojene temperature tališča smo uporabili računalniški program za določanje termodinamskih lastnosti TAPP (slike 17 do 20). S pomočjo programa smo določili okvirne sestave frit, ki bi jih lahko uporabili. Glede na naše zahteve je proizvajalec ponudil 6 frit, katerih delež kristalne faze smo določili z rentgensko praškovno analizo (slike 30 do 35). Glede na dobljene rentgenograme smo frite razdelili v tri skupine:

- frito R1 z delom $SiO_2$ v kristalni strukturi,
- friti R2 in R3 z večjim deležem $SiO_2$ v kristalni strukturi,
- frite R4, R5 in R6, ki so imeli v celoti steklasto strukturo.

**Oblikovanje skoznika**

Zaradi zahtev po boljši mehanski vzdržljivosti skoznika smo izvrtali luknjo v obliki konusa (slike 28 in 29a, b) z vrhom, ki je bil obrnjen proti zunanjosti ohišja (minimalna površina skoznika je izpostavljena telesu). Površina tako izdelanega konusa je dejanska površina medfaznega sloja Macor/frita. Če primerjamo površino klasične izvrtine s konusno, je slednja v našem primeru večja za 21 krat pri enaki debelini ohišja. Kakovost tako izdelanega skoznika je neprimerno večja, v strokovni literaturi pa te enostavne rešitve nismo zasledili.

**Postopek zatalitve skoznika**

Postopek zatalitve skoznika je bil narejen po principu dobre laboratorijske prakse. Postopek zatalitve je po priporočilih proizvajalca Macor keramike vseboval naslednje faze:

- struženje (Litostroj Potisje, Ada, Srbija) ohišja in pokrova stimulatorja s fino končno obdelavo
- vrtanje lukenj za skoznik s prirejenimi svedri za dosego ustrezne geometrije z vrtalnikom Black & Decker power drill KR753 (Stanley Black & Decker, Stanley Drive, USA)

- čiščenje pribora in pripomočkov pred uporabo je potekalo deset minut v ultrazvočnem čistilcu Branson 2510 (Branson Ultrasonic corporation, Danbury, USA) z deionizirano vodo. Sledilo je splakovanje z deionizirano vodo, acetonom in zračno sušenje
- čiščenje frit: pred vsakim ciklom zataljevanja se je frite čistilo enako kot čiščenje pribora
- sušenje frit: po čiščenju so se frite sušile dve uri na 200 °C v univerzalni sušilni peči (Kambič SP-45C)
- mletje frit: za prvo in drugo serijo vzorcev so se frite ročno zmlele v ahatni terilnici, za tretjo in četrto serijo pa strojno v napravi Retsch PM100 (Retsch GMBH, Haan, Germany) z uporabo YSZ kroglic
- priprava Pt žic: za posamezni skoznik so se uporabile žice dolžine 10 mm in preseka 0,3 mm. Sledilo je oblikovanje žic v črko L.
- zapolnitev skoznikov s fritami: za posamezno serijo so se hkrati izdelali skozniki na enem kosu Macor keramike. Vzorec keramike je bil postavljen na delovno mizo tako, da so bili vrhovi izvrtin usmerjeni navzdol (oblika kraterja), v katere se je namestilo Pt žice. Luknje se je zapolnilo tako, da je bila zgornja površina sloja frit poravnana s površino keramike. Ker se pri stabilizaciji Pt žic ni uporabila nobena priprava, je bilo potrebno postopek zapolnjevanja večkrat ponoviti, ker je prišlo do zamaknitve posameznih žic
- zataljevanje frit je potekalo v laboratorijski peči Protherm PFL 100/3 (Alserteknik, Sokak, Turkey) po različnih programih (grafi 1-4)
- pri drugi seriji se je cikel zazaljevanja ponovil dvakrat. Vsakič se je na posamezni strani skoznika dodalo manjkajočo količino frite, da bi dosegli polno zapolnitev luknje skoznika
- pri prvi seriji skoznikov se je na zunanjo stran keramike z metodo termičnega naparevanja v vakuumski komori chamber (Pfeiffer Vacuum, Asslar, Germany) nanesla Pt debeline nanosa okoli 150 nm, na notranjo stran pa plast Ti debeline 650 nm s pomočjo elektronskega curka (Thermionics laboratory, Inc, Hayward, USA)

- žarjenje za odpravo notranjih napetosti je potekalo pri 700 °C v času 15. minut s hitrostjo segrevanja in ohlajanja 3 °C/minuto.

**Izdelava skoznikov**

Izdelali smo štiri serije skoznikov, kot prikazuje tabela 10. Skupno vsem serijam je uporaba oksidativne atmosfere ter hitrost segrevanja (4 °C/minuto) in ohlajanja (1 °C/minuto).

**Analize frit in skoznikov**

Frite smo analizirali z rentgensko praškovno analizo (Panalytical X`pert PRO MPD, Panalytical B.V., Almelo, The Netherlands). Glede na rentgenograme smo frite razdelili v tri skupine, kasnejše analize pa so to enostavno razdelitev načeloma potrdile.

Skoznike smo analizirali z optično mikroskopijo (Nikon Eclipse E20 (Nikon Corporation, Tokyo, Japan), opremljen s kamero Infinity 1 ter pripadajočo programsko opremo software (Lumenera Corporation, Ottawa, Canada) pri povečavi 40x in 100 x. Za natančno mikro analizo smo analizirali vzorca R6-S1 (slike 61 do 70) in R6-S2 (slike 71 do 76) z vrstičnim elektronskim mikroskopom ter opravili elementarno analizo (EDX) na vzorcu R6-S1 (slike 77 do 82).

Z optično mikroskopijo smo kot najprimernejši friti za izdelavo skoznika opredelili friti R4 in R5. Sledila je frita R6, ki smo jo izbrali za elektronsko analizo. V primeru, da bi elektronska mikroskopija pokazala primernost frite R6 za izdelavo skoznika, bi to hkrati pomenilo tudi primernost frit R4 in R5.

**Rentgenska analiza**

Frite smo razdelili v tri skupine (slika 31) glede na obliko rentgenograma oziroma vsebnost kristaliničnih faz:

- frita R1
- friti R2 and R3
- frite R4, R5 and R6

**Optična mikroskopija**

**Prva serija**

Pri prvi seriji izdelave skoznikov je zatalitev Pt žice potekala pri 900 °C (graf 1). Rezultati niso bili takšni, kot smo pričakovali. Frita R1 se je zgolj natalila, pri nekaterih (friti R2 in R3) je bila težava v le delnem zalitju luknje skoznika (slike 36 do 43). Pojavila se je poroznost, ki je bila sicer prisotna tudi v vseh nadaljnjih serijah.

Pred pričetkom izdelave skoznikov smo testirali zataljevanje Pt žice neposredno z Macor keramiko z uporabo pulznega laserja. Rezultati so pokazali smiselnost uporabe te tehnologije v zaključni fazi. Tako smo pri prvi seriji skoznikov na notranjo stran ohišja naparili Ti (slika 36), zunanjo pa s Pt (slika 37). Debelina Ti prevleke je bila 650 nm ter platinaste okoli 150 nm.

**Druga serija**

Postopek zataljevanja pri drugi seriji (graf 2) je bil najprimernejši za popolno zatalitev Pt žice. Rezultati zatalitve vseh frit so primerljivi (slike 44-50). Pri tej seriji se je frito zataljevalo trikrat, z dodajanjem frite v drugem in tretjem ciklu se je kompenziralo poroznost in delno omočljivost. S tem načinom smo dosegli popolno zatalitev skoznika.

**Tretja serija**

Temperaturni diagram tretje serije je vseboval izoterme pri 800 °C v času 1h pri segrevalnem in ohlajevalnem ciklu (graf 3). Pri tej seriji nas je zanimalo, če procesi difuzije pri 800 °C (mejna temperatura neprekinjene uporabe Macor keramike) vplivajo na izoblikovanje spoja (slike 51 do 55). Poleg tega smo za tretjo in četrto serijo frite strojno zmleli na velikost okoli 1 mikrona, kar naj bi imelo za posledico zmanjšanje poroznosti. Izkazalo se je, da enakomerna velikost delcev v našem primeru ni idealna za zmanjševanje poroznosti v zataljenih fritah. Z optično mikroskopijo ni bilo mogoče oceniti smotrnost uvedbe izoterm pri 800 °C. Delež poroznosti je večji kot pri ročnem mletju vzorcev. Pri tej seriji z optično mikroskopijo ni opaziti zelo fino porazdeljene poroznosti, kar nakazuje na termodinamično bolj aktivno zataljevanje frit.

**Četrta serija**

Rezultati zadnje serije so podobni kot pri tretji, v zataljenih fritah je bil prisoten velik delež poroznost, pri tem pa tudi znotraj te serije ni vidne fine porazdeljenosti (slike 56-60). Friti R2 in R3 sta pri teh pogojih zalili celoten volumen skoznika.

**Elektronska mikroskopija**

Elektronska mikroskopija (slike 61 do 76) je pokazala, da je oblikovanje medfaznega sloja na fazni meji Macor/frit zvezno brez nepravilnosti v mikrostrukturi. Širina medfaznega sloja je vsaj 50 µm, kjer je aktivna difuzija posameznih elementov borosilikatne faze keramike in frite. Tudi omočenje Pt žice je popolno. Zaključimo lahko, da je skoznik hermetično zaprt, stopnjo hermetičnosti pa bo potrebno izmeriti.

## Zaključek

Zatalitev Pt žice v keramično ohišje implantabilnega dela stimulatorja je zelo pomembna, pa vendar le ena izmed faz izdelave nevromuskulatornega stimulatorja. Potrebno bo izvesti številne teste preden bomo lahko z gotovostjo dejali, da je

implantabilni del varen za uporabo v človeškem telesu. Na začetku dela smo imeli možnost uporabe različnih materialov za zalivko, ki pa se je že v začetni fazi zožila predvsem zaradi razpoložljive opreme. Tehnologija izdelave skoznika s frito kot zalivnim materialom se je izkazala za primerno. Pri tem sta bila najboljša rezultata dosežena s fritama R4 in R5 v drugi seriji s tremi cikli zataljevanja (tabela 11).

Načeloma so vse frite dobro omočile površino Macor keramike in Pt žico ter so primerne za našo aplikacijo z izjemo frite R1, ki pri zgoraj opisanih pogojih zataljevanja ni primerna. Glede na opravljene analize je tališče te frite višje od 1000°C, s čimer pa do nastanka medfaznega sloja ne pride.

Poroznost spoja je problematična, vendar se jo da odpraviti z dodatnimi vmesnimi fazami pod vakuumom.

Hermetičnost je pogojena s samim materialom. Pri implantabilnemu delu stimulatorja je problematičen medfazni sloj Macor/frita in omočenje Pt žice s frito v skozniku. Nepravilnosti na teh mejah kot so poroznost, nezvezen prehod, vključki in ipd. povzročajo notranje napetosti in pospešujejo ionski tok.

Rezultati pilotne serije so pokazali, da je predstavljena tehnologija primerna za izdelavo skoznika, pri tem pa je potrebno uvesti dodatne faze v procesu zataljevanja (odprava poroznosti, zaključno lasersko varjenje), da bi dosegli zahtevano kakovost skoznika.

**Nadaljevanje razvoja**

Razvoj skoznika je aktiven proces. Naslednji korak je izdelava ddruge generacije skoznika, ki vključuje odpravo poroznosti in lasersko zataljevanje notranje in zunanje površine skoznika s čimer se bo zaprla površinska poroznost in s tem povečala hermetičnost.

Po končani fazi izdelave skoznika so na vrsti testiranja biokompatibilnosti, hermetičnosti in mehanskih lastnosti. Merjenje prebojnega toka bo dalo prvo informacijo o kakovosti skoznikov.

Ker je izdelava skoznikov dala dobre rezultate, obstaja možnost, da uporabnost prenesemo na področje izdelave senzorjev. Osvojeno znanje in visoka dodana vrednost teh proizvodov sta dobri motivaciji za razvoj in izboljšave.

# Contents

# 1 Introduction

We are now at the beginning of the 21st century and health is one of the most important assets in our life. In most countries a public health service is provided to every individual. Being ill, physically unaesthetic or disabled nowadays does not mean necessarily struggling in life. But it has a lot of meaning in social situations and how society accepts those individuals. Often it can happen that they are pushed aside in society and treated as a marginal group.

Through our human history man has tried to restore and maintain health using the knowledge and technology that was available at that time. It is only after middle of the last century that technology was developed in such a way that it was possible to carry out systematic work on so called biomaterials. In order to restore a part or a function in a body certain devices are needed. Those devices must be made out of materials that are safe and reliable and used according to purpose.

In the public health care system services are generally provided in the field of implanted medical devices. In the private sector there is an emphasis on aesthetic surgery. It is estimated, that almost in every 17 people in developed countries has a device of some kind implanted in the body. This also provides a financial reason for the huge development in the field of implanted devices, biomaterials and connected industries.

One type of implanted device is a neuromuscular stimulator [1-4] (implantable gait corrector). The essential part of this device is the implanted unit. The weakest part of this unit is the feedthrough. The feedthrough must provide a leakage – free seal, combining usually two or more different materials (ceramic/metal, ceramic/ceramic, metal/metal, glass/metal, etc.) to ensure adequate mechanical properties in bearing all kind of loads while it is functioning.

Detailed analysis and investigations of all involved materials in a device is needed to answer if it is completely safe in performing its intended function in a human body. We must not forget that while the patient is using implant, in order to improve his or hers health, for the human body the same implant is just a foreign body placed in a harsh environment. If biotolerance is to be within limits, the human body ideally

accepts the implant otherwise it will be rejected. Carefully selected materials and procedures for manufacturing of the implant unit form a solid base for successful implementation.

# 2 Implantable medical devices

To use implanted devices in quantities as we do today, certain technology development is needed. Within the last 60 years there has been huge development in the field of biomaterials; we are still only at a beginning. The biological processes and parts of the body that have either direct or indirect contact with an implant are not fully understood. The prediction of successful implantation is difficult and is one reason why new materials are slowly determined as being biocompatible. Nevertheless, new fields in medicine are using new implants in order to improve health e.g. tissue engineering or nerve stimulation in the case of epilepsy. New approaches and new materials are introduced on the time for improved performance.

## 2.1 Materials

The key criterion for material selection is how it behaves in the human body. Although the prime selection criteria for materials is done by looking at basic limitations like biocompatibility, mechanical properties and field of application, we are still left with variety of possible candidate materials. One can choose proven technologies from the past or go with new material for the future. The trend right now is to use materials with very similar properties to those of the parts or organs being replaced in the body (chemical composition, mechanical properties) and which is a recent development. In the case of total hip prosthesis replacement, metal is often chosen, but because of its high strength it passes load to weaker parts – in this case to surrounding bones. By using a material with similar properties to bones this negative effect of implantation can be eliminated.

### 2.1.1 Type of biomaterials

A wide range of materials [5-7] are used as biomaterials in medical application:

- metals
- polymers
- ceramics
- composites
- glasses
- carbons
- biomimetics (natural biomaterials)

Table 1: Some ceramic materials in medical applications [8]

| Ceramic | Chemical Formula | Comment |
|---|---|---|
| Alumina | $Al_2O_3$ | Bioinert |
| Zirconia | $ZrO_2$ | |
| Pyrolytic carbon | | |
| Bioglass | $Na_2OCaOP_2O_3–SiO$ | Bioactive |
| Hydroxyapatite (sintered at high temperature) | $Ca_{10}(PO_4)_6(OH)_2$ | |
| Hydroxyapatite (sintered at low temperature) | $Ca_{10}(PO_4)_6(OH)_2$ | Biodegradable |
| Tricalcium phosphate | $Ca_3(PO_4)_2$ | |

Definitions:

*Bioinert* refers to a material that retains its structure in the body after implantation and does not induce any immunologic host reactions.

*Bioactive* refers to materials that form bonds with living tissue.

*Biodegradable* refers to materials that degrade (by hydrolytic breakdown) in the body while they are being replaced by regenerating natural tissue; the chemical by-products of the degrading materials are absorbed and released via metabolic processes of the body.

Ceramics (table 1) [8] are the most versatile materials and can have different roles in a human body. They can be used as bioinert, bioactive or biodegradable materials. Metals (table 2) [8] on other hand are suitable in general as bioinactive materials. Problems associated with using metals come from the release of ions into the human body with undesirable consequences. Metals are chosen mostly because of their superior mechanical properties. Alloys are preferable; the pure metals used are for examples precious metals and Ti.

Table 2: Chemical composition of commonly used metal alloys [8]

| Element | 316L Stainless Steel (ASTM F138,139) | Co–Cr–Mo (ASTM F799) | Grade 4 Ti (ASTM F67) | Ti-6Al-4V (ASTM F136) |
|---|---|---|---|---|
| Al | — | — | — | 5.5–6.5 |
| C | 0.03 max | 0.35 max | 0.010 max | 0.08 max |
| Co | — | Balance | — | — |
| Cr | 17.0 | 26.0–30.0 | — | — |
| Fe | Balance | 0.75 max | 0.30–0.50 | 0.25 max |
| H | — | — | 0.0125–0.015 | 0.0125 max |
| Mo | 2.00 | 5.0–7.0 | — | — |
| Mn | 2.00 max | 1.0 max | — | — |
| N | — | 0.25 max | 0.03–0.05 | 0.05 max |
| Ni | 10.00 | 1.0 max | — | — |
| O | — | — | 0.18–0.40 | 0.13 max |
| P | 0.03 max | — | — | — |
| S | 0.03 max | — | — | — |
| Si | 0.75 max | 1.0 max | — | — |
| Ti | — | — | Balance | Balance |
| V | — | — | — | 3.5–4.5 |
| W | — | — | — | — |

Table 3: Polymers separated according to performed tasks [8]

| Applications | Polymer(s) |
|---|---|
| Cardiovascular implants | Polyethylene; poly(vinyl chloride); polyester; silicone rubber; poly(ethylene terephthalate); polytetrafluoroethylene |
| Orthopedic implants | Ultra-high-molecular-weight polyethylene; poly(methyl methacrylate) |
| Drug release | Poly(lactide-co-glycolide) |
| Tissue engineering | Poly(lactic acid); poly(glycolic acid); poly(lactide-co-glycolide) |

The use of polymers (table 3) [8] in biomedical technology is focused on the development of specific tasks like dialysis and controlled drug delivery.

### 2.1.2 Implants and their medical use

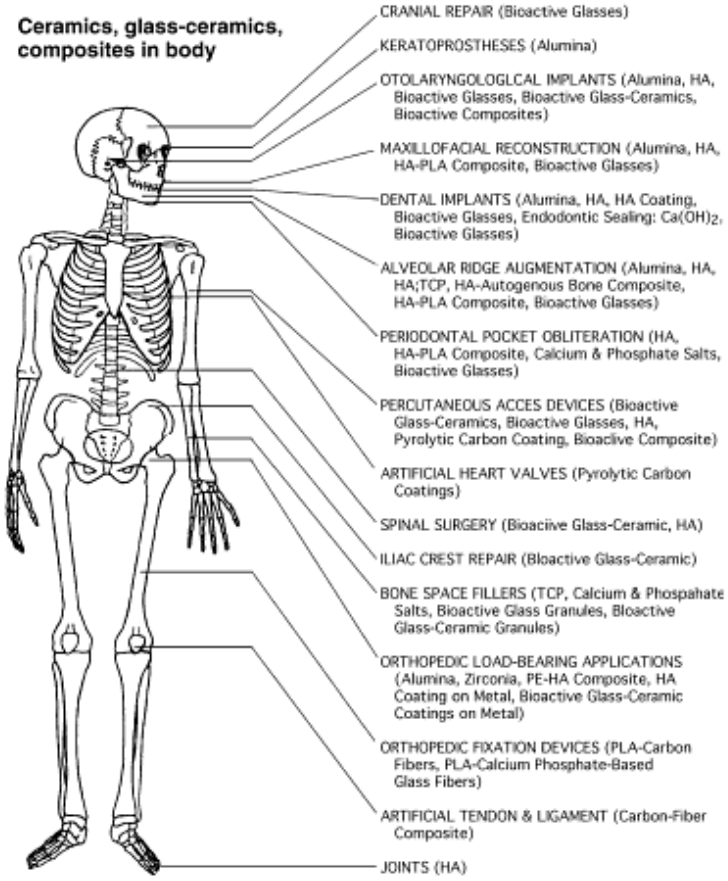


Figure 1: Clinical uses of bioceramics [9]

Biomaterials are used in medicine (figure 1) [9, 10] in the fields of [5, 10]:

- orthopedics
- cardiovascular applications
- ophthalmics
- wound healing
- dental applications
- drug-delivery systems
- plastic surgery
- sutures

## 2.2 Biocompatibility

Callan stated "A biomaterial is any substance (other than a drug), synthetic or natural, that can be used as a system or part of a system that treats, augments, or replaces any tissue, organ, or function of the body; especially, material suitable for use in prostheses that will be in contact with living tissue" [11]. Biomaterials science is interdisciplinary: it can involve knowledge of metallurgy, chemistry, physics, biology, mechanical engineering, electricity and electronics, medicine, pharmacy and many more. When biomaterials are in contact with living tissues and inner body fluids interactions occur. These interactions are occurring both ways; the material is having an impact on the human body and vice versa.

When impacts are qualified as non-destructive the material is biocompatible.

A few subjects must be discussed when referring to materials used in human body [12]:

- biocompatibility
- toxicology
- healing
- functional tissue structure and pathobiology
- specific shapes
- mechanical and performance requirements
- ethics
- regulations

When referring to biocompatibility the following terms should be used:

As Savich stated "*Bioinactivity* is the state of implant material in which there is no living tissue response to the material and the implant itself determined by instruments or histologically or noticeable effect of tissues and fluids that would change the microstructure and deteriorate the mechanical properties of the material...

*Biotolerance* is the property of implant material owing to which any reactions of living tissues are endured by the human body without serious inflammatory processes and the effect of tissues and fluids on the material does not cause the

intoxication of the body with corrosion products, wear, catastrophic changes in microstructure, or deterioration of the mechanical properties that does not permit the proper function of implants" [13]. Oxides are bioinactive while the metals are not. Noble metals and stainless steels are biotolerant.

Bioinactivity and biotolerance are combined into the term biocompatibility.

In reality we cannot speak about bioinactivity - there are always some sort of interaction between the implanted material and living tissue.

Long term success of implantation depends on [13] engineering (material, manufacturing, surface and inner structure, design) and medical factors (peculiarities of the patient's body, professionalism of operation):

## 2.3 Hermetic packaging

Hermeticity can be described as the state or condition of being airtight [14]. In the real life we cannot achieve 100 % hermeticity in the long term. Depending on the method of encapsulation all materials are permeable to some degree (figure 2) [15].

In the case of an encapsulated implant device, the inner body fluids can penetrate through feedthrough which is the starting point for leakage. This can cause the malfunction of inner electronic circuit. In addition these body fluids can then circulate back to the surface of the device, carrying ions of different metals from within; this can be toxic to the body. This process can also be accompanied by deterioration of the implanted materials, surface electrical leakage or electrical shorts. In the 2006 auditory reliability report it was stated that almost 75 % of these devices failed due to moisture ingression.

To achieve hermetic sealing often sophisticated techniques are used such as laser welding, electron beam welding, TIG and infrared laser beam.

The degree of hermeticity depends on the [15]:

- material,
- feedthrough/seal design,
- technique used,
- environment

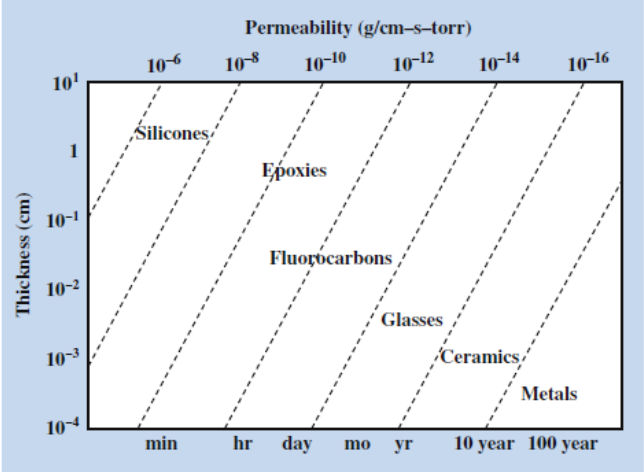


Figure 2: Permeability of different materials depending on thickness and time [15]

Figure 2 [15] shows the dependency of permeability with time, material type and thickness. The most suitable materials (in terms of permeability) according to this figure are metals followed by ceramics and glasses. This property of a material is directly related to the nature of the bonding in the atoms and molecules. The preferable are metallic followed by covalent and covalent-ionic bonds.

## 2.4 Testing methods for implanted medical devices

The construction of medical implant must met different conditions and demands that may appear during usage and as well during manufacturing, transportation and storage [15].

### 2.4.1 Biocompatibility tests

By far the most complex tests are done in biocompatibility studies [15]. More and more tests are done "in vitro", but still some medical applications demand extensive in vivo animal experiments. In this case permission for the studies is granted by the National medical ethics committee. All the tests are made according to ISO 10993 series (20 standards) prior to a clinical study. Within those standards details for individual tests are not given. In general most tests deal with different kinds of toxicity.

### 2.4.2 Hermeticity tests

After biocompatibility hermeticity is most important factor. There are different standards [15] covering that area, such as MIL_STD-883. Standard ASTM F979-86/2003, a standard test method for hermeticity of hybrid microcircuit packages prior to lidding, was withdrawn in 2009. Most techniques use a helium leakage test and the value that divides a fine leaker from a gross one is $1*10^{-5}$ atm-cc/sec of air.

### 2.4.3 Material characterizations

Material characterization [15] begins with optical microscopy. The next step is scanning electron microscopy (SEM/EDX) where can we combine great magnification and elemental information on all formed phases. Tomography of surface can be also examined with atomic force microscopy (AFM). Further sophisticated characterizations are X-ray diffraction (XRD), transmission electron microscopy (TEM, STEM) and more. The above methods can give information's about material structure and phases within. This is solid base for all studies on biomaterials since properties come from structure of the material.

### 2.4.4 Mechanical tests

Implanted devices are fixed in a body in different ways. However, they do move along with bones and tissue that surrounds them. Some implants must withstand significant mechanical forces (artificial hip joints) and mechanical tests [15] show if the implant is appropriate for the task. The following tests are the most common in assuring proper quality not only after implantation, but also in production, surgery, etc.; tensile, fatigue, vibration, compression, shock and flexural testing. Regarding environmental stability, stability testing can include temperature cycling, humidity and corrosion.

### 2.4.5 Corrosion tests

Our implant is designed in such way, that there is a very little possibility for corrosion processes to occur. However, the inner electronic circuit and feedthrough are spots, where the corrosion can appear. Electrochemical impedance spectroscopy

(EIS) and cyclic voltammetry (CV) are part of standard testing [15]. ASTM standards G5-94 and G106-89 describe all methods for corrosion determination.

## 2.5 State of the art in biomaterials

The term "biocompatibility" has been for the first time mentioned in journal in year 1970 (1300 times in year 2007) [16]. Scientists are working systematically on so called biomaterials and biocompatibility only for a half of century. At this point of view it is not surprising that a tremendous development is today in the field of materials for medical applications. Until now the main development has been made in the clinical use of medical implants and other devices [8, 17]. Development and researches made within are reflecting on novel materials that will be even safer, reliable and that they won't act as foreign body (proactive biomaterials). Studies revealed [18] that biocompatibility is better when material is acting similar to surrounding tissues and cells instead of being passive or inert. Proactive biomaterials elicit desired response to surrounding tissues and cells, specific to their task [19]. Mainly, those are surface coatings [18, 20-22] to promote desired relationship between implanted material and the human body. Those materials can be found i.e. in tissue and cellular engineering [23] at a molecular/genetic level.

In science is very common that materials developed for specific task found during time alternative usage. Same is valid for biomaterials. Today novel material for treating and curing diseases can be tomorrow used within implanted unit.

It is not important only chemical composition of materials but also structure of materials. Future development is going from microstructured to nanostructured materials [24, 25] which can meet more demanding physical, chemical and mechanical criteria for material selection. In addition, future trends go toward minimization [26-28] which is a huge challenge in engineering and manufacturing.

### 2.5.1 Biomaterials for implanted devices

Most commonly used materials in medical implants are metals and ceramics, but some novel plastic materials [29-31] are also to be found as appropriate.

Metals are still prime choice for stimulating electrodes and wires since they conduct electricity. Following metals and alloys are tested/used among others:

- Pt based alloys: Pt [3, 32, 33], Pt-Ir [26, 34-36],
- Fe based alloys: Fe–22Cr–10Ni–6Mn–2Mo–0.4N [37], 316L stainless steel [37], medical grade stainless steel [36, 38]
- Ti based alloys: β-type Ti-14Mo-3Nb-1.5Zr [39], α-type Ti-10Zr [39], α-type CP (commercially pure) Ti [39], Nitinol (TiNi) [24]
- others: Ta [28], MP35N (CoCrNi) [36]

The housing (case or package) material for implanted unit can also be made from various kinds of materials, preferably from metal or ceramic. Ceramic housings are needed if the signals or energy have to be transmitted (RF frequency) otherwise metals can be used [40].
Some of materials for housing are listed below:

- ceramics: alumina [36, 40, 41], Yttria stabilized zirconia [42],
- metals: α-type CP (commercially pure) Ti [38], Nb [38, 40], Ta [28, 38], stainless steel [40], CoCr alloys [40]

Critical and thus important points of implanted units are feedthroughs, sealing and encapsulating of the housing.
In encapsulating technology plastic materials are preferred in case when there is no demand for hermeticity; epoxy based plastics [36], acrylate based plastics [40], medical grade silicone [3, 36], polyimides [15], silicon-carbons [15], poly(ethylene oxide) based plastics [22] and novel high performance liquid crystal polymers (LCP) [15] are some of possible choices.

### 2.5.2 Feedthrough assembly

Feedthroughs in implanted units are connecting housing with stimulating electrodes and antennas through wires. Depending on a design, feedthrough purpose is to seal together two materials; metal with metal, ceramic with metal, glass with metal, etc. To make a hermetic seal, proper material should be choosing as sealing material. It is a hard task to choose the right one, since it must connect two usually quite different materials regarding physical and chemical properties. Furthermore, seal must withstand all kind of loads during usage and at the same time form hermetic barrier.

We must keep in mind, not that all used materials for feedthrough manufacturing, but also formed ones must be biocompatible. This is important aspect, since it is common that sealing temperatures are of 1000 °C or more. Newly formatted phases on materials borders can possess different properties than expected. Many times it is reflecting as leakage and degradation when implant comes in touch with body liquids.

Common materials as sealants are:

- metals (are used mostly when ceramic part is between metal housing and metal pins): 99,99 % Au brazed alloy [43]
- glasses: borosilicate glass [26, 28]

We have two options regarding feedthrough in implanted unit; we can manufacture it or we can buy it.

The main reasons why we should manufactured it:

- we know what materials are used within (GLP guidance)
- designing freedom, we choose design, materials and technology
- if we buy feedthrough we still need to connect it with a housing
- if we buy feedthrough, materials within are sometimes unknown (trademark, patent pending, etc.)

Main reasons why we should buy it:

- feedthroughs are extensively tested, hermeticity and biocompatibility are proofed
- durable and reliable design

There are a lot of companies that are producing feedthroughs for various applications including medical or are specialized in the medical field; some are listed:

- Greatbatch medical, Clarence, USA
- SCT (solutions in ceramic technology), Bazet, France
- Morgan Technical Ceramics Alberox, Bedford, USA
- PAVE Technology Company, Dayton, USA

## 2.6 Implantable gate corrector: an overview

The work in this thesis is based on the first generation of implantable gait corrector manufactured by Itis, d.o.o. Ljubljana and it is described in this chapter. The case materials for implanted unit – Macor ceramic for housing and Pt for wires were the same; also the design of the implanted unit was not changed. This chapter presents assembly and functioning of the first generation of implantable gait corrector. Three devices from the first generation were implanted in the patients [2]. The pilot study of the second series aimed for improved durability of the feedthrough in order to provide long-time hermetic enclosure.

The implantable gate corrector [3] is used for correction of drop-foot by stimulating the common peroneal nerve (CPN). Selective stimulation of muscles tibialis anterior (TA) and the peroneus brevis (PB) contribute to strong dorsal flexion and moderate eversion of the foot is achieved with a stimulating electrode installed on the nerve behind the lateral head of fibula.

### 2.6.1 Principles of functioning of implantable gait corrector

The IGC is assembled [3] of different parts located outside and inside of the human body. The main principles in its function are as follows: to determine the phase of the gait, the heel switch on the shoe (figures 3b, d) is activated and it sends the signals through an external unit (figure 3c) to the electronics in the implantable unit (figure 20a). Signals are transferred to the cuff with monopolar platinum electrode for stimulation of the CPN. This nerve stimulates TA and PB muscles to restore their function and thus allowing the hemiplegic patient to walk.

### 2.6.2 Assembly of IGC

#### 2.6.2.1 External part

The external parts of IGC (figure 3) [3] are:

- external stimulator (figure 3a)
- heel switch (figure 3b)

- external unit attached on the leg of the patient (figure 3c)
- gait of the patient with stimulation (figure 3d)

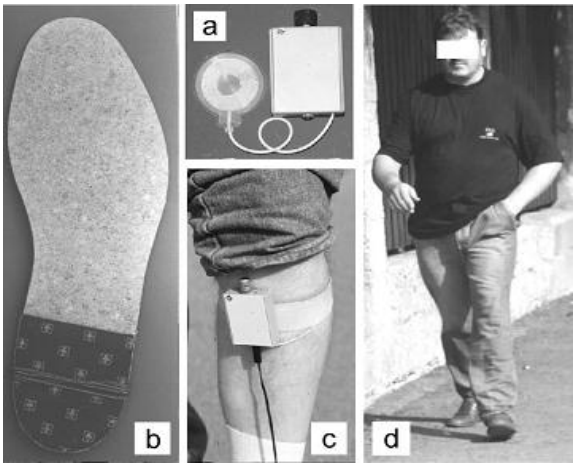


Figure 3: External parts of the implantable gait corrector [3]

#### 2.6.2.2 Implantable unit

The implanted unit (figure 4) [3] is composed from following parts:

- housing
- electrode on housing of the stimulator
- platinum wire
- stimulating electrode

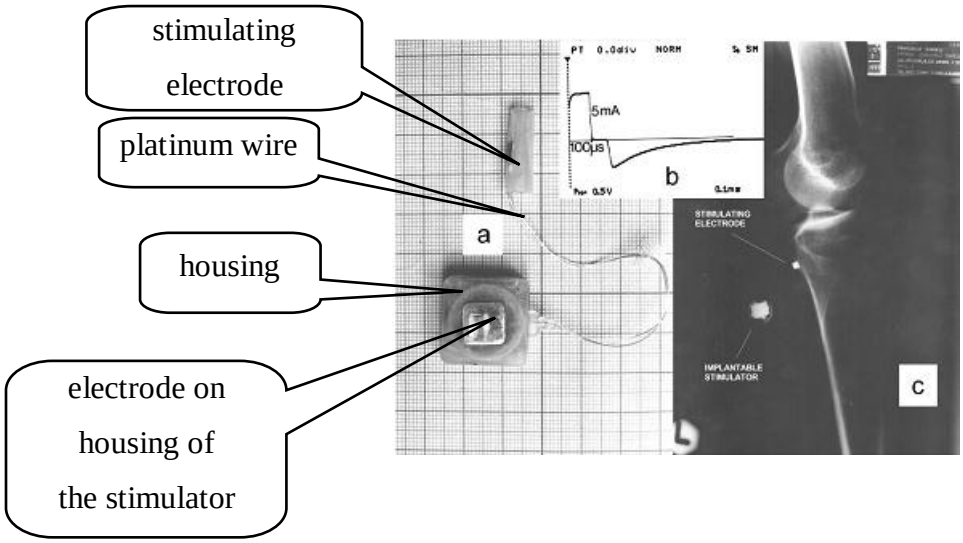


Figure 4: The implanted unit, stimulating pulse and X-ray of the implanted unit [3]

In figure 4a [3] are presented parts of implantable unit, in figure 4b pulse for stimulating nerves and X-ray (figure 4c) of the implanted stimulator with stimulating electrode showing its position on the CPN behind the lateral head of the fibula.

The ceramic housing has two feedthroughs for platinum wires [3]. The feedthrough on the side of the housing enables transfer of impulses through the platinum wire on the cuff with stimulating electrode installed on the CPN behind the lateral head of the fibula. The feedthrough on the bottom of the housing leads to the neutral electrode attached on the housing of the implanted unit. In the housing is installed a passive receiver which receives the signal, converts it and sends to the electrode with a carrier frequency of 2 MHz. Macor ceramic provides a transparent radio frequency window. The whole housing is encapsulated in a polymer.

The bulk body of an implantable unit is a block with dimensions of 9x22x22 mm carrying thick hybrid electronic circuitry and feedthroughs to the stimulating electrodes. The use of ceramic is reasonable due to non-metallic encapsulation (RF transmission) and long service life after implantation. Hybrid electronic circuitry was designed in a way to enable hermetically packaging and covering by a ceramic lid. Obtained single-side hermetically encapsulated hybrid electronic circuitry and receiving antenna were then enclosed in the ceramic housing and lid. The dimensions of the implant body were determined by molding disc-shaped ceramic (Macor ceramic) in medical grade silicone in vacuum unit.

# 3 Chemical bonds and formation of microstructure in ceramics and glasses

The feedthrough is the crucial part of an implant unit. It is the major source of leakage and subsequent malfunctions of inner electronics and/or implant rejection. The problem lies in the function of the feedthrough. In our case it connects ceramic and metal and the seal must compensate for the tensions in the material caused by thermal expansion. Furthermore it must withstand constant dynamic, tensile and torsion stresses since the patient is in constant movement and the Pt wire attached to the implanted body must do the same. For these reasons the seal must provide excellent mechanical connection with both materials – ceramic and metal. It must also be designed in such a way that it wets the metal forming reliable bonds and at the phase boundaries with the ceramic is able to form stable biocompatible phases.

## 3.1 Chemical bonds

In materials there are different chemical bonds which are formed as consequence of nature of bonding in atoms. In ceramics we can have larger number of elements combined and the nature of bonds is usually covalent-ionic which makes these materials structurally very complex.

### 3.1.1 Covalent bonding

When two atoms are sharing at least one pair of electrons we describe the bond as a covalent bond. It can be either as molecular substance or it can form 3D covalent networks. Molecular substances with weaker bonds have much lower melting points than covalent network solids. In ceramics we often find covalent network bonding and some elements that form it, particularly often are Si, B and C. Some example of materials with network bonding are $SiO_2$ (figure 5) [44] and diamond.

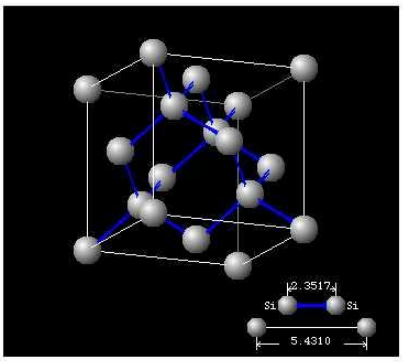


Figure 5: $SiO_2$ structure with covalent bonds (blue) [44]

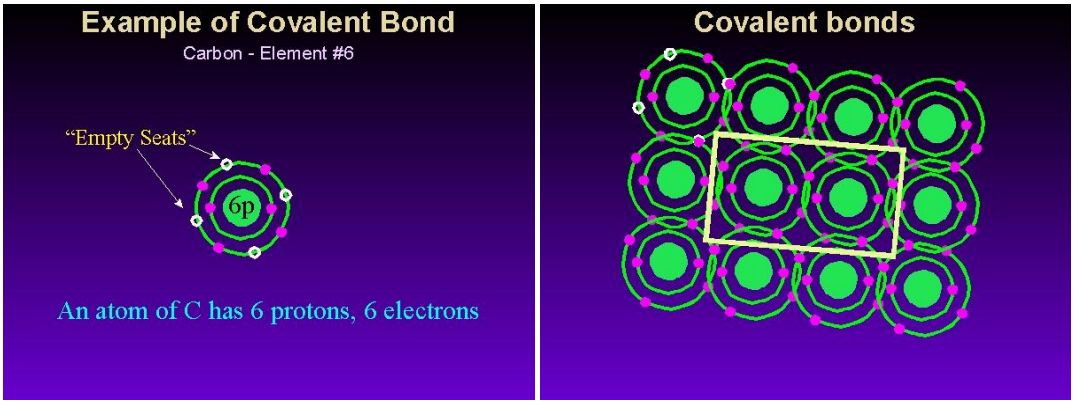


Figure 6: Shared electrons in diamond structure forming a covalent bond [44]

When describing covalent bonds Lewis diagrams (figure 7a) [45] are mostly used, but they can mislead, especially in 3D presentations since the formed bond angle is not always 90 ° or 180 °.

As an example the structure of methane will be explained [45]. Carbon has an electronic configuration of $1s^2 2s^2 2p_x^1 2p_y^1$ (figure 7b) [45]. Actually it has 2 unpaired electrons to share with, instead of the 4 (Lewis diagram). In the bond are involved outer electrons (figure 7b) since $1s^2$ electrons are too far from neighboring atom. There are only two 2p electrons available for sharing. When bonds form, energy is released resulting in a more stable system. When carbon forms 4 bonds instead of 2, twice as much of energy is released and system becomes even more stable. Because of the small energy gap between the 2s and 2p orbitals only a small amount of energy is needed for one electron to overcome the energy gap and thus forming 4 unpaired electrons (figure 7c) [45]. Since the electron is in higher position it is excited. 4

unpaired electrons now forming identical bonds but they are in two different orbitals so they rearranging electrons in a process called hybridization when they form identical hybrid orbitals $sp^3$ (figure 7d) [45]. The newly formed orbitals are equally distanced from each other. When joining with hydrogen again new orbitals with 2 electrons are formed but now with a hydrogen nucleus embedded in each lobe (figures 7e, f) [45]. The scheme is same as that of Lewis diagrams and principle can be applied to any covalent bond molecule.

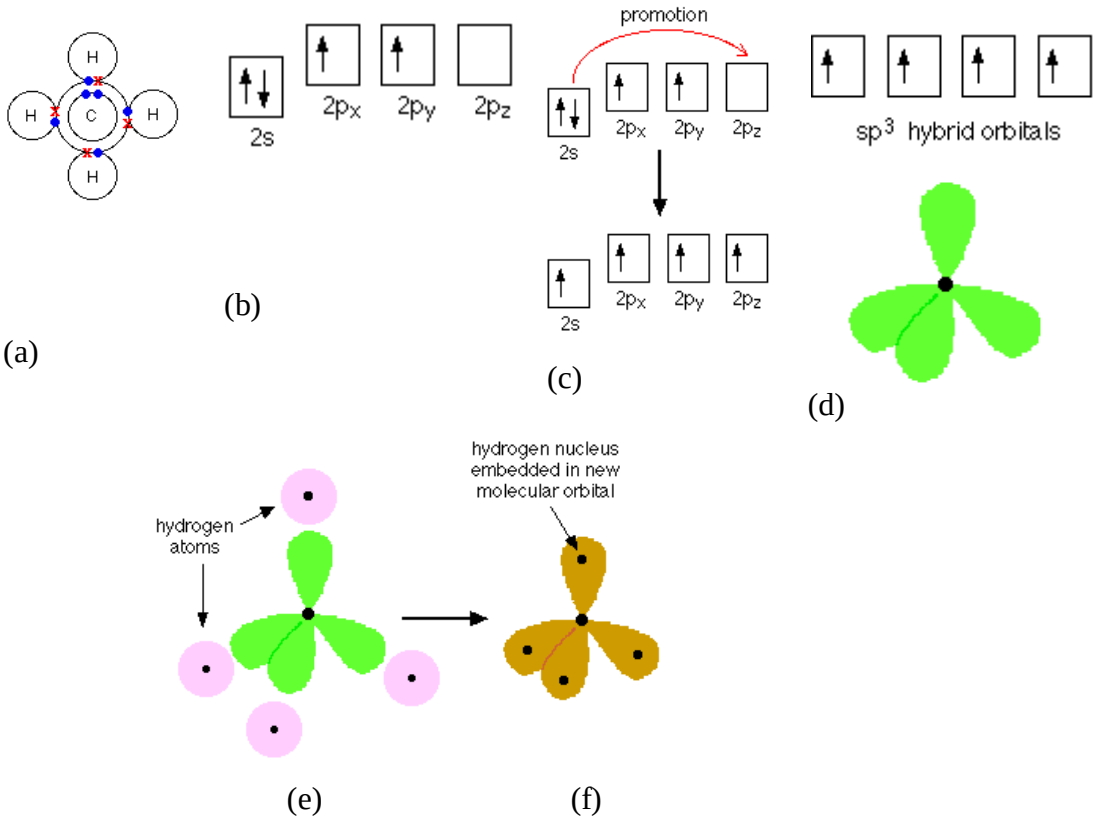


Figure 7: Covalent bonding in methane [45]

### 3.1.2 Ionic bonding

- also called electrovalent bonding appears between two elements having large difference in electronegativity (figure 8) [46] as a result of transfer of the valence electron from the element with low electronegativity to the element with high electronegativity. Exchanging of electrons is made in a way that outer orbits are either completely full or completely empty. The more electrons which are exchanged the stronger is the bond.

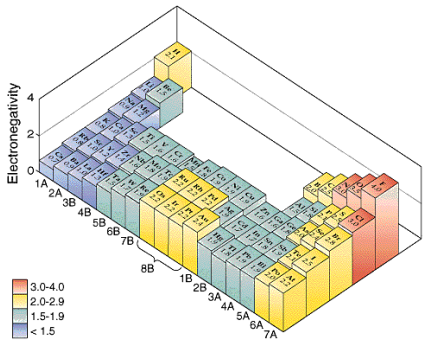


Figure 8: Periodic table showing electronegativity of elements [46]

In the case of Mg and O [47], Mg is giving 2 electrons to O becoming $Mg^{2+}$ and oxygen becomes $O^{2-}$. Magnesium oxide (figure 9) [47] which is formed when magnesium burns in oxygen is held together by very strong attractions between the ions.

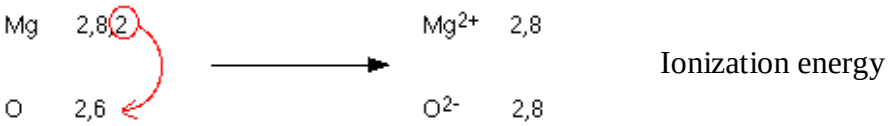


Figure 9: Formation of ionic bond in MgO [47]

Materials with ionic bonds have high melting points and boiling temperatures, they don't conduct electricity in a solid but they are conductive in liquid state. They are often found as hard and brittle materials.

### 3.1.3 Covalent-ionic bonding

Ceramics can be quite complex multiphase materials with a mixture of covalent and ionic bonds [48].

The share of ionic bonds (IB) [49] can be calculated from the following equation:

$$IB = \exp(-0.25*\Delta E^2) \qquad \text{(eq. 1) [49]}$$

where:

**IB** – share of ionic bonds,

**ΔE** – difference of electronegativity of the elements.

Table 4: Metal oxides and bonds found within [48]

| oxide | $z/(r_c+r_a)^2$ | share of ionic bonds (IB) | coordinate number (CN) solid - liquid | type of oxide |
|---|---|---|---|---|
| $Na_2O$ | 0,18 | 0.65 | 6 6-8 | alkaline oxides (network destroyers) |
| BaO | 0.27 | 0.65 | 8 8-12 | |
| CaO | 0.35 | 0.61 | 6 | |
| MgO | 0.48 | 0.54 | 6 | |
| $Al_2O_3$ | 0.83 | 0.44 | 6 4-6 | amphoteric oxides |
| $TiO_2$ | 0.93 | 0.41 | 4 | |
| $SiO_2$ | 1.22 | 0.36 | 4 | acidic oxide (network creator) |

$r_c$ – radius of the cation

$r_a$ – radius of the anion

rc/ra = 0.732…1.0 (BaO) CN = 8, cubic structure

rc/ra = 0.414…0.732 (CaO, MgO) CN = 6, octahedral structure

rc/ra = 0.225…0.414 ($SiO_2$) CN = 4, tetrahedral structure

## 3.2 Formation of microstructure

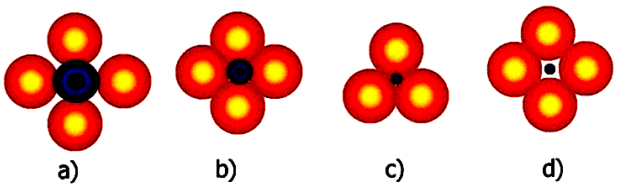


Figure 10: Stable structures (a, b, c) and an unstable one (d) depends on rc/ra ratio [48]

The incorporation of an anion in crystal structure of cations (figure 10) [48] can be stabilizing or destabilizing (rc/ra factor) (figure 11, table 5). Thermodynamically all systems tends toward stable conditions which demand minimum energy for existence.

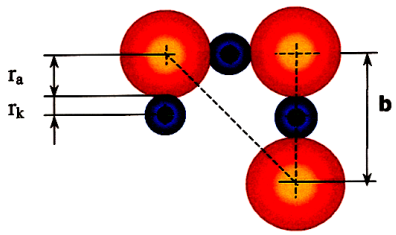


$b = 2\,(r_k + r_a)$, $\quad b = \frac{4 * r_a}{\sqrt{2}}$

$r_k = 0{,}414 * r_a$

Figure 11: Geometric conditions of interactions of cations and anions in crystal structure [48]

Table 5: Radii of some cations and anions [48]

| cations | $Si^{4+}$ | $Al^{3+}$ | $Fe^{3+}$ | $Mg^{2+}$ | $Fe^{2+}$ | $Mn^{2+}$ | $Ca^{2+}$ |
|---|---|---|---|---|---|---|---|
| $r_c$ (nm) | 0,041 | 0,050 | 0,060 | 0,065 | 0,075 | 0,080 | 0,093 |
| anions | $F^-$ | $O^{2-}$ | | | | | |
| $r_a$ (nm) | 0,136 | 0,140 | | | | | |

### 3.2.1 Glass formation

Certain elements and compounds are able to form glassy structures (table 6) [9]. Among those are $SiO_2$ and $B_2O_3$. Since the glass is formed only at certain conditions it is less thermodynamically stable that a crystalline phase. To change it into the crystalline state it only requires enough thermal energy for a defined period of time.

Table 6: Materials that can be made into glass [9]

| Category | Examples |
|---|---|
| Elements | S, Se, P |
| Oxides | $B_2O_3$, $SiO_2$, $GeO_2$, $P_2O_5$, $As_2O_3$, $Sb_2O_3$, $In_2O_3$, $Tl_2O_3$, $SnO_2$, $PbO_2$, $SeO_2$, |
| Sulfides | $As_2S_3$, $Sb_2S_3$ |
| Carbonates | $K_2CO_3$–$MgCO_3$ |
| Polymers | PMMA[a], PS[b], PVC[c] |
| Metallic alloys by "sprat cooling" | $Au_4Si$, $Pd_4Si$ |

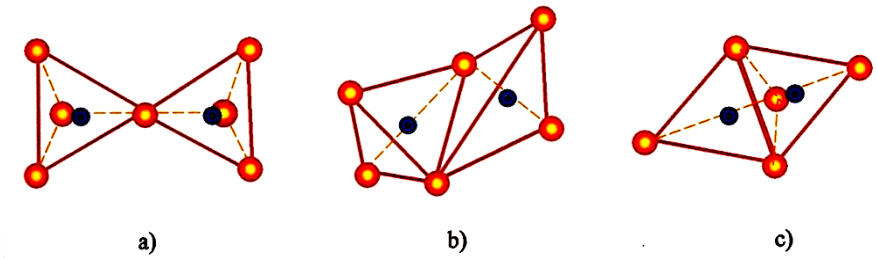


Figure 12: $SiO^{4-}$ tetrahedrons can be bonded together in different ways [48]

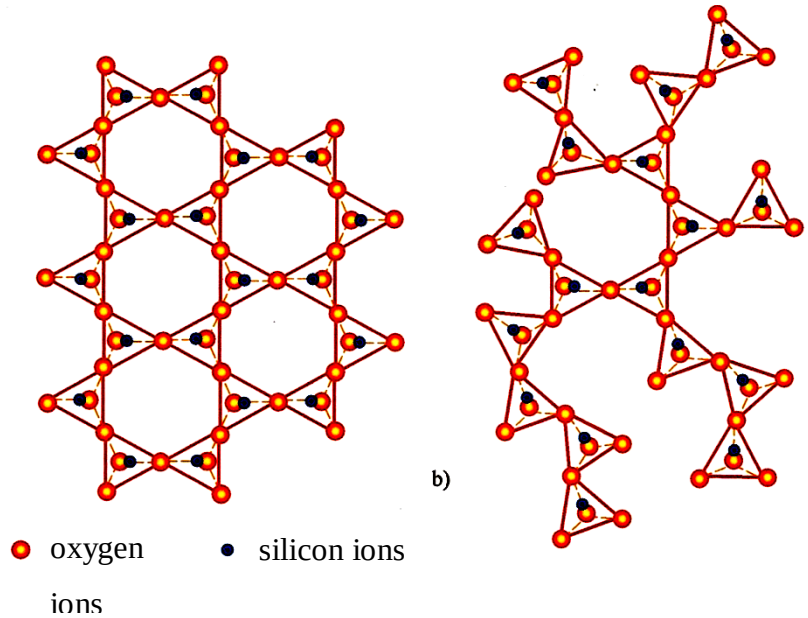


Figure 13: 3D network of silica tetrahedrons in solid is starting to disintegrate during remelting [48]

Silica primarily has covalent bonds. If tetrahedrons of $SiO^{4-}$ are bonded with an oxygen ion, a 2D or 3D network is formed (figures 12a and 13a) [48]. This structure is not close coupled and thus the density is low. Because the tetrahedra have long-range order the structure is crystalline.

The rate of crystallization is directly related to the rate of glass formation (figure 14) [9] . With a high speed of translation (around 10 milliseconds) it is not possible for crystals to grow larger than 100 Å and so a glass forms.

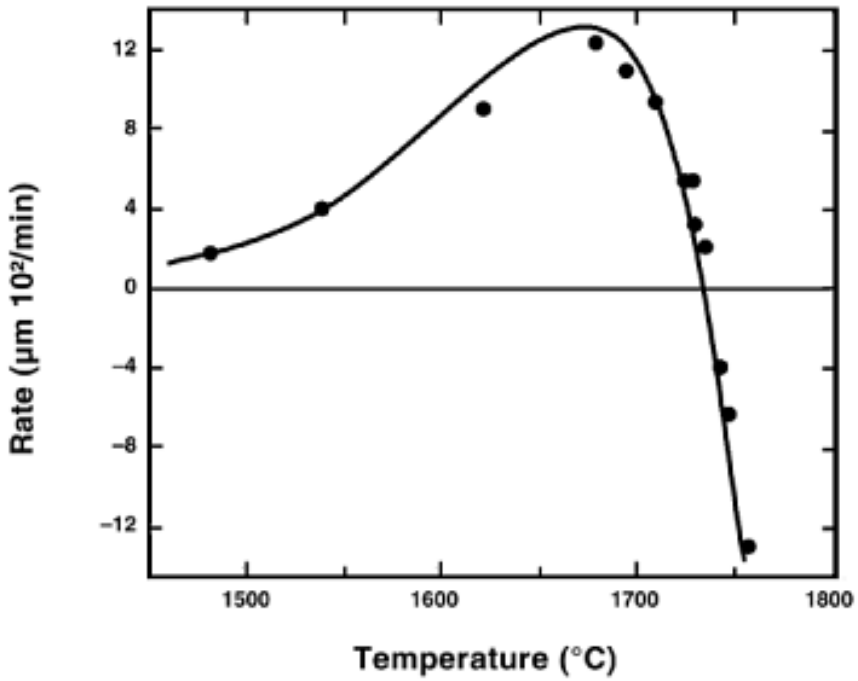


Figure 14: Rate of crystallization of Cristobalite ($SiO_2$) from fused silica [9]

$\nu = H_f (T_m - T) / (3 \pi a^2 \eta T_m)$ (eq. 2) [9]

where:

$H_f$: heat of fusion at the melting point,

a: the lattice spacing,

η: viscosity of the liquid.

According to equation 2 [9], high viscosities close to melting point ($T_m$) will result in glass formation (table 7) [9]. A low melting temperature and an asymmetric molecular structure will generally form glasses more readily.

Table 7: Rate of crystallization, temperature and viscosity [9]

| Material | $T_\alpha$ (°C) | Maximum velocity (cm/s) | Temperature at max. velocity (°C) | Log viscosity at $T_\alpha$ (P) |
|---|---|---|---|---|
| $SiO_2$ | 1734 | $2.2 \times 10^{-7}$ | 1674 | 7.36 |
| $GeO_2$ | 1116 | $4.2 \times 10^{-6}$ | 1020 | 5.5 |
| $P_2O_5$ | 580 | $1.5 \times 10^{-7}$ | 561 | 6.7 |
| $Na_2O–2SiO_2$ | 878 | $1.5 \times 10^{-4}$ | 762 | 3.8 |
| $PbO–2B_2O_5$ | 774 | $1.9 \times 10^{-4}$ | 705 | 1.0 |
| Glycerol | 18.3 | $1.8 \times 10^{-4}$ | –6.7 | 1.0 |

For oxides 3D aperiodic networks with energy comparable to that of the crystal network will favor glass especially at following conditions [48]:

- An oxygen atom is linked to a maximum two glass-forming atoms
- The coordination number (CN) of the glass-forming atoms is small (table 4)
- The $SiO^{4-}$ polyhedrons are bonded via an oxygen ion (figure 12a)
- The $SiO^{4-}$ polyhedrons form a 3D network

A consequence of 3D network formation is usually high viscosity which propagates glass formation (low rate of crystallization) and having high bonding energy between O and M atoms (>80 kcal/mol). A low heat of fusion additionally lowers nucleation rate and crystal growth and thus promotes glass formation.

In the case of a $SiO_2$ network (figure 15a) [50] other atoms can incorporate within structure (figures 15 and 16) [50] or can exchange with the Si atom in tetrahedra resulting in changed chemical and physical properties. If the structure becomes distorted, amorphous $SiO_2$ glass is formed (figure 15b) [50] and the network becomes modified. $Na_2O$ and CaO can be added to lower very high glass transition temperature ($T_g$).

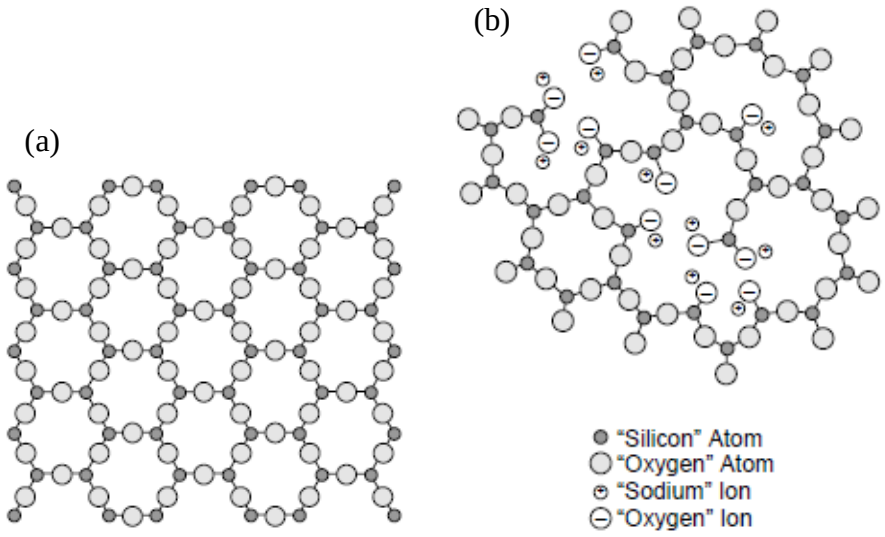


Figure 15: Incorporation of Na atoms and effect on network formation [50]

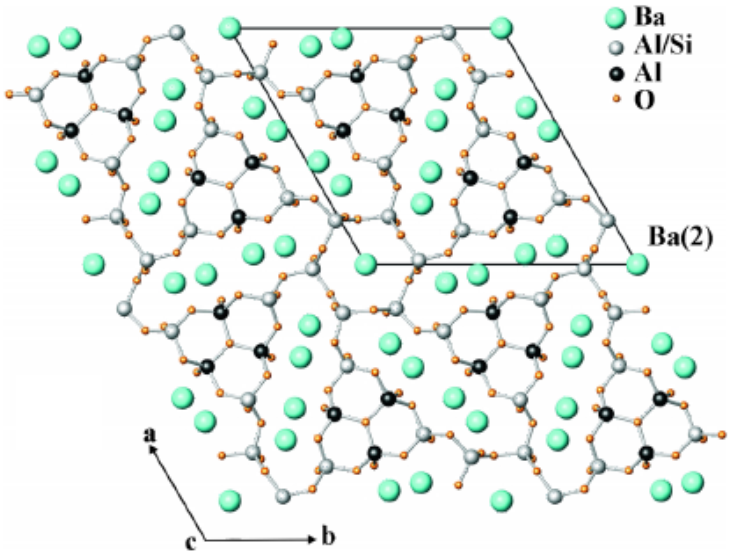


Figure 16: Incorporation of Ba and Al ions in $SiO^{4-}$ polyhedrons [51]

To change the structure and properties it is usual that other ceramics are added and mixed together [12, 51]. Remelting and solidification result in new alloys and compounds (microstructure constituents).

## 3.3 Phase diagrams

We use phase diagrams for determination of phase transformation during heating or cooling. Phase diagrams are collected in so called "atlases" or in software tools like TAPP or Thermo-Calc. These tools are essentially materials property and phase diagram databases. Data sources and coefficients are used to calculate temperature/pressure-dependent properties.

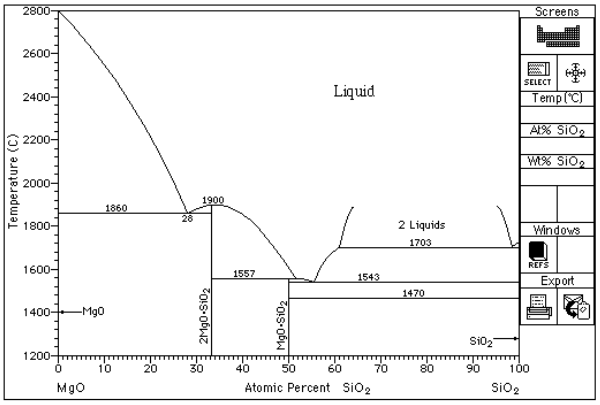


Figure 17: Binary phase diagram MgO-$SiO_2$ with eutectic systems

In figure16 we see that two eutectics are able to be formed; at temperature 1860 °C (28 at. % $SiO_2$) is formation of MgO-2MgO*$SiO_2$ and at second eutectic point in system (1543 °C) when the formed eutectic is MgO*$SiO_2$-$SiO_2$.

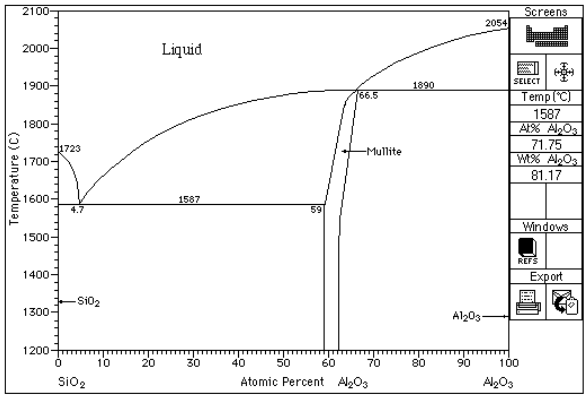


Figure 18: Binary phase diagram $SiO_2$-$Al_2O_3$

In the binary phase diagram $SiO_2$-$Al_2O_3$ (figure 17) a eutectic is formed consisted from $SiO_2$ and Mullite (3Al2O3*2$SiO_2$ or 2$Al_2O_3$*$SiO_2$) at 4.7 % $Al_2O_3$ and 1587°C.

The system is used in high temperature applications for bricks, ladles, sample holders, insulating material, etc.

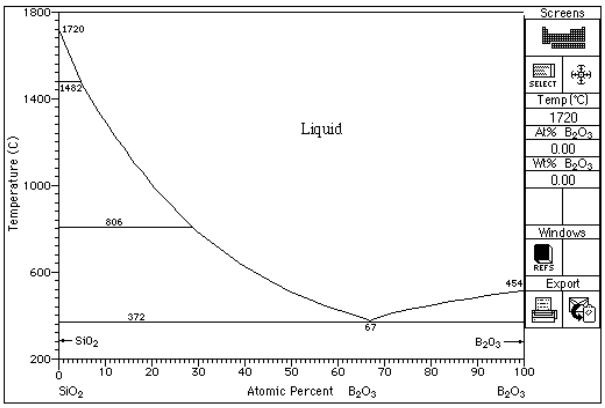


Figure 19: Eutectic system $SiO_2$-$B_2O_3$

Addition of $B_2O_3$ (figure 18) to $SiO_2$ significantly lowers the liquidus temperature. Again, a eutectic system is formed with the eutectic reaction at 67 % $B_2O_3$ and 372°C. $B_2O_3$ has a vitreous form. It is used in production of borosilicate glass and other applications such as a fluxing agent, additive or catalyst.

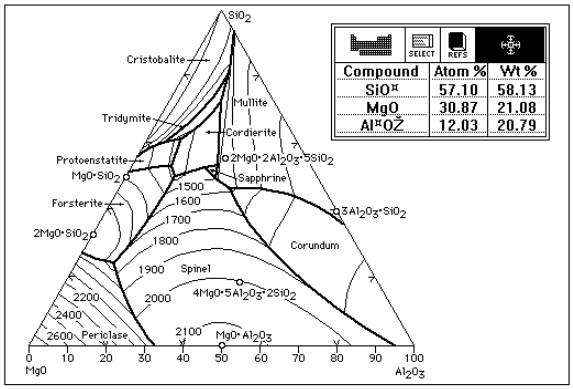


Figure 20: Ternary phase diagram $Al_2O_3$- $SiO_2$-MgO

A ternary phase diagram (figure 19), the phases with lowest liquidus temperatures are Cordierite and Tridymite (1400 °C).

With powerful software tools like TAPP or Thermo-Calc and appropriate databases we can in an initial step of selecting appropriate material and chemical composition, choose optimal materials.

# 4 Experimental

## 4.1 Material selection

When we designed implanted unit of second generation, we had two aspects in mind; first, the success of the first generation gait corrector [3] and second, available equipment to perform experiments. For that reason we preselect Macor ceramic and Pt for manufacturing a feedthrough. A study goal of a second generation pilot series was to find appropriate material and technology to fuse Pt wire in Macor ceramic housing. Thorough study regarding possibilities, knowledge and available equipment point us to frits as prime choice as the bonding material. For that matter we chose carefully selected frits from company Emo Frite d.o.o., Celje, Slovenia.

One of the important materials properties of the feedthrough build in materials is thermal expansion. Pt (8.8 μm/mK [52]) is a metal that has a very low thermal expansion coefficient and is similar to the Macor ceramic with coefficient of 9.3 μm/mK [53-55] (borosilicate glass has 3.3 μm/mK [56]).

Conductivity is another important thermal property. While Macor is 1.46 W/mK [53-55], Pt reaches 71.6 W/mK [52]. The seal is formed with a frit whose purpose is to compensate different physical properties of surrounding materials and thus strengthen the bondage between them.

## 4.2 Housing and the lid

For the housing and the lid of the stimulators the ITIS d.o.o. Ljubljana, Slovenia, uses machineable ceramic commercially named Macor which had proved in the past to be excellent material for this application for housing implants [3]. A further reason why it was chosen by ITIS d.o.o., Ljubljana, lies also in the excellent machining capability using standard metalworking tools. To produce material (ceramic) in any shape in your own shop gives you advantage in crafting. In addition the expenses are lower and it is less time consuming. Secondly, because it is ceramic, radio frequency communication between the external and implanted unit is possible. This means there is no need to place receiving antenna outside of the implanted unit.

Materials that have micro-crystals of mica ($KMg_3AlSi_3O_{10}F_2$) in a borosilicate glass matrix ($SiO_2$-$B_2O_3$-$Al_2O_3$-$K_2O$-MgO-F) [57] are Macor ( developed by Corning Glass Work Inc. [55]) and Photoveel (developed by Sumimoto Photon Ceramics Co., Ltd) [58]. Using a multiphase material with different and separate functions of crystalline and glassy phases gives better results than single phase silicate glass. The glassy phase provides appropriate relaxation properties while crystalline phase allows long term stability.

Macor (figure 21) [53-55] is porcelain like glass ceramic composed of 55 % of fluorphlogopite mica in a borosilicate glass matrix [53-55]. It has excellent thermal characteristics and is stable up to temperatures of 1000 °C (at 800 °C of continuous usage). It is material with very little thermal expansion and outgassing. The property that makes this glass ceramic unique is also zero porosity. It is a proven material in medical applications and aerospace technologies.

The chemical composition of Macor is generally [53-55]: 46 % $SiO_2$, 17 % MgO, 16 % $Al_2O_3$, 10 % $K_2O$, 7 % $B_2O_3$ and 4 % F. Borosilicate glass is composed of about 81 % $SiO_2$, 13 % $B_2O_3$, 4 % $Na_2O$ + $K_2O$ and 2 % others [59].

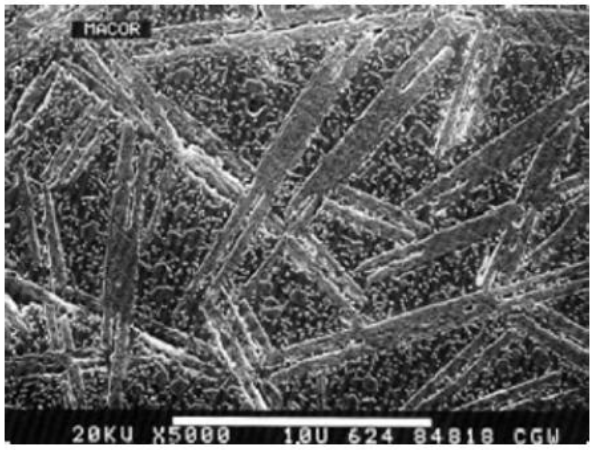


Figure 21: Microstructure of Macor (SEM 5000x) [53-55]

The source of fluorphlogopite mica [60] is crude mica – a naturally formed underground ore. It is a silicate consisting of phlogopite and muscovite. The chemical composition is $KAl_2$ $(AlSi_3O_{10})(OH)_2$ and $KMg_3(AlSi_3O_{10})(OH)_2$.

Fluorphlogopite Mica is formed when remelted in a platinum pot below 1500°C with $F^-$ (fluorine) replacing hydroxyl $(OH)^-$.

The properties of fluorphlogopite mica that make this material so unique [60]:

- thermal expansion is very low (fig. 22) [60]
- has superior stability of heat (fig. 23) [60]. Up to 1100℃, the thickness would be unchanged; decomposition will gradually start at 1200℃. Its melting or crystallization temperature is 1350±5 ℃.
- The vacuum deflation (fig. 24)[60] is low, only absorbed gases such as $O_2$ , $N_2$ and Ar
- as no outgassing (vapor of $H_2O$) material, it is recommendable as electric vacuum insulant
- is not inclined to distortion and can bear high stress, tension and compression forces
- will not react with common acid and alkali solutions

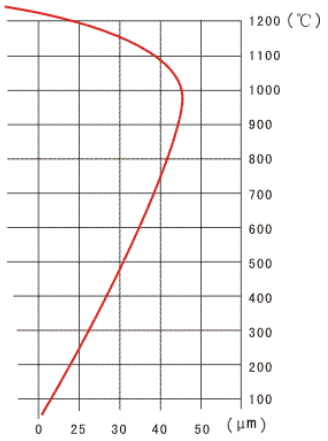


Figure 22: Thermal expansion of fluorphlogopite mica [60]

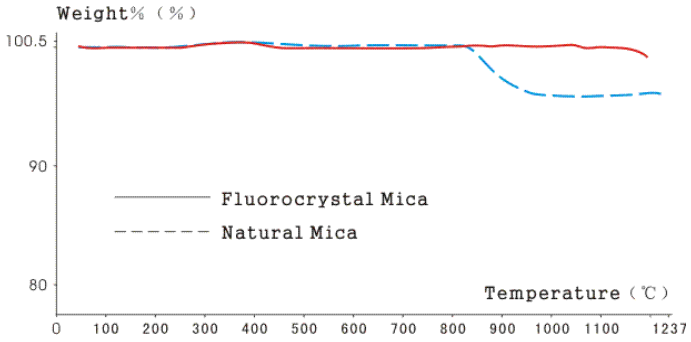


Figure 23: Thermogravimetry (TG) of natural and fluorphlogopite mica [60]

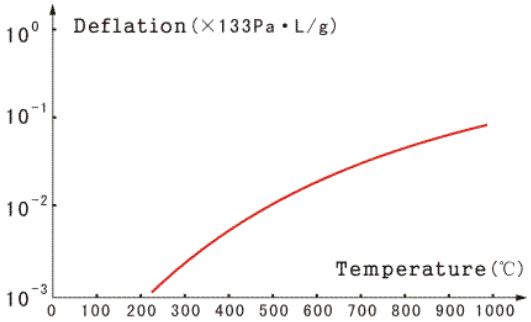


Figure 24: Deflation (TG) of fluorphlogopite mica [60]

To form a feedthrough using macor ceramic [54] a variety of fabrication procedures can be employed from simple to sophisticate. Macor ceramic can be bonded to other materials or to itself in numerous ways including [54]:

- soldering
- brazing
- co-firing
- straight mechanical joints

We used fusion (co-firing) under oxygen (air) atmosphere as it is the most appropriate sealing technology regarding selected sealing materials.

## 4.3 Stimulating electrodes and the wires

Pt wire is used because platinum is biocompatible and chemically stable over a wide potential range and therefore is a good choice for implantable electrodes. Desirable Pt properties are a result of non-oxidibility and high melting temperature – these are reasons why platinum has been used along with glass for sealing in industry and science equipment since the 19$^{th}$ century.

Platinum wire of thickness 0.3 mm was used as pins in the feedthroughs. It was chosen because of bioinactivity – research by ITIS d.o.o. revealed that there were no reactions with surrounding tissue in earlier implants [61-63]. Electrodes were for the same reason the same material. Pt and frits do not form interphases at the contact surface. The mechanical strength of the junction is for that reason not strong.

## 4.4 Frits

In the table below are the chemical compositions of individual frits with phases that are same as in Macor ceramic. The frits are commercially available at Emo Frite, d.o.o., Celje, Slovenia but the company does not want to public disclose chemical compositions of the frits. In general the frits are in glassy state but there can be also small share of microstructure constituents in crystalline state (figures 30 to 34).

Table 8: Chemical composition of individual frits

| | | | | | | | | | | | |
|---|---|---|---|---|---|---|---|---|---|---|---|
| nr. | material | $SiO_2$ | $Al_2O_3$ | $Na_2O$ | $K_2O$ | $B_2O_3$ | CaO | MgO | $TiO_2$ | BaO | $F^-$ |
| | | | | | | | | | | | |
| 1 | frit R1 | x | x | x | x | x | x | x | | | |
| 2 | frit R2 | x | x | x | x | x | x | x | | | |
| 3 | frit R3 | x | x | x | x | x | x | x | | x | |
| 4 | frit R4 | x | x | x | | x | x | | | | |
| 5 | frit R5 | x | x | x | x | x | x | | | | |
| 6 | frit R6 | x | x | x | x | x | | | x | | x |
| | Macor | x | x | ! | x | x | ! | x | | | x |

After debates [64], literature study [65-73] , patents study [74-88] and previous work [3] we select frits as bonding material. The basic requirement was to achieve bonding below 1000 °C at which temperature is the limitation of usage of Macor ceramic. In light of those conditions the chosen materials were frits with dominantly glassy phase (XRD analysis). A further demand was that constituents (oxides) would be generally the same as in Macor but with different compositions (table 8). Determination of $T_m$ (melting point), $T_g$ (glass transformation temperature) and $T_f$ (furnace temperature) (figure 25)[89] in glassy or crystalline phases is connected to the chemical composition and bonding mechanism (figure 26)[89]. Since we expected that in seal formation would be primarily involve the glassy phase of Macor (borosilicate glass) the chemical composition of frits was thus targeted, but also included alumina and magnesia for higher strength.

Oxides that are present in the frits and Macor are following:

- $SiO_2$, $Al_2O_3$ and $B_2O_3$
- $K_2O$ is present in all frits except R4
- MgO is in frits R1, R2 and R3
- $F^-$ and $TiO_2$ are presented only in R6 frit
- $Na_2O$ is in all frits
- CaO is in all frits except in R6 frit
- BaO is found only in frit R3
- $TiO_2$ is found only in frit R6

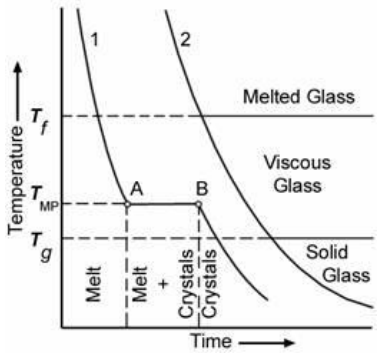


Figure 25: Temperatures of liquid-solid transitions of crystalline material and glass [89]

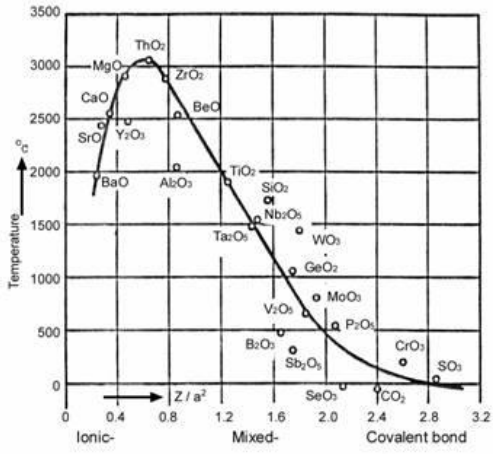


Figure 26: Dependency of chemical bonds with strength of the seal ($Z/a^2$) and melting point ($T_m$) [89]

## 4.5 Feedthrough series

Although the feedthroughs were made in the same way, there were some variations (table 9). The base was a frit sealing in a laboratory furnace Protherm PLF 100/3 (Alserteknik, Sokak, Turkey) with an oxidative atmosphere. With variations in the manufactured series we tried to set optimal parameters for seal formation (end temperature, grinding/particles size, number of sealing cycles). Maximum use temperature of Macor ceramic is determined at 1000 °C. Although it would be preferred to fuse the frits at higher temperatures we manufactured our series at 900 °C and 1000 °C.

Table 9: Variations in the feedthrough series

| feedthrough series | max. temp. (°C) | no. of heating/cooling cycles | isothermal step | grinding | metal coating |
|---|---|---|---|---|---|
| 1st | 900 | 1 | no | manual | Pt/Ti |
| 2nd | 1000 | 3 | no | manual | no |
| 3rd | 1000 | 1 | at 800 °C/1h | machined | no |
| 4th | 1000 | 1 | no | machined | no |

### 4.5.1 Series 1

Frits were prepared in a mortar by manual grinding. The size distribution with this kind of preparation is wider and the grains are generally larger. For all series the heating rate (4°C/minute) and cooling rate (1 °C/minute) were the same. For all series we heated up the samples to desired temperature without isothermal steps at maximum temperature. In the first series the highest temperature was 900 °C (chart 1).

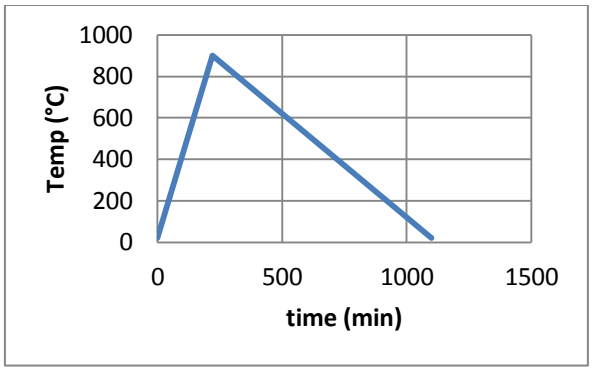


Chart 1: Temperature diagram for the 1st series

For the next step – laser sealing, deposition of metals was made on surface of the crucible. For the outer side, Pt deposition was chosen. Since the pin in the feedthrough is made out of the same material there should be no chemical potential between those two. Corrosion is therefore not expected in this respect. Thin Pt layer would be enough for laser sealing of the seal surface and thus make more difficult for inner body fluids to penetrate through the seal. On the other side, a layer of pure Ti was deposited.

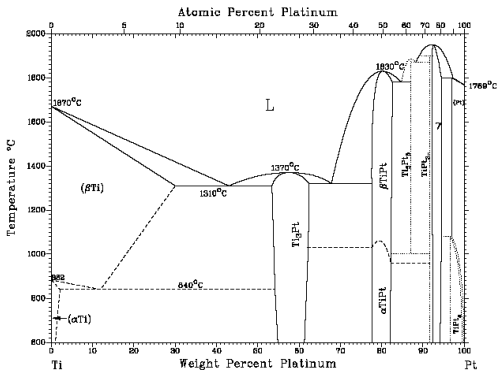


Figure 27: Pt-Ti binary phase diagram [90]

In figure 27 [90] is shown the calculated Pt-Ti phase diagram . It was expected that on the interphase of Pt/Ti some low temperature phase could be formed such as $Ti_3Pt$, TiPt or $TiPt_8$ [90]. It is known that corrosion resistance of pure Ti is improved with addition of the Pt and Pd. Highest improvement is achieved by adding 1- 3 % of Pt and the formation of TiPt [90].

### 4.5.2 Series 2

The increase in heating temperature to 1000 °C (chart 2) was done because it was expected that with higher temperature the diffusion of the frits will increase enabling more air to be expelled. This cycle was repeated three times; when the frits were added to the inner and outer part of the seal to compensate for volume loss during remelting. Due to higher sealing temperature, better interphase formation was expected because of increased atom migration.

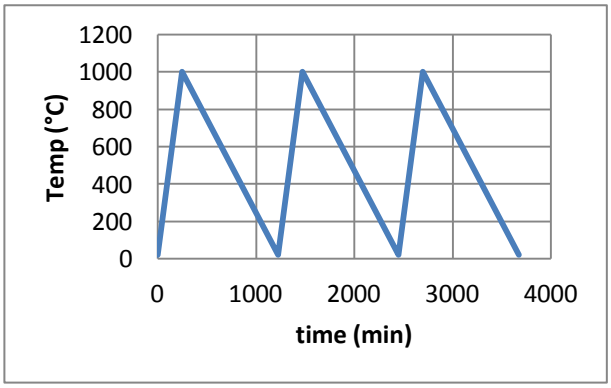


Chart 2: Temperature diagram for the 2nd series

### 4.5.3 Series 3

For the third series (chart 3) frits were ground in a planetary balls mill Retsch PM100 (Retsch GMBH, Haan, Germany) with the following procedure: total time of 1 hour with rotating speed of 350 rpm, YSZ balls were used and acetone was added as a grinding promoter. A uniform grain size of about 1 micron should lower the amount of trapped air during seal preparation, thus helping to achieve lower porosity. The maximum frit sealing temperature was the same as in second series (1000 °C) so results could be compared and the effect of grain side evaluated in term of seal formation.

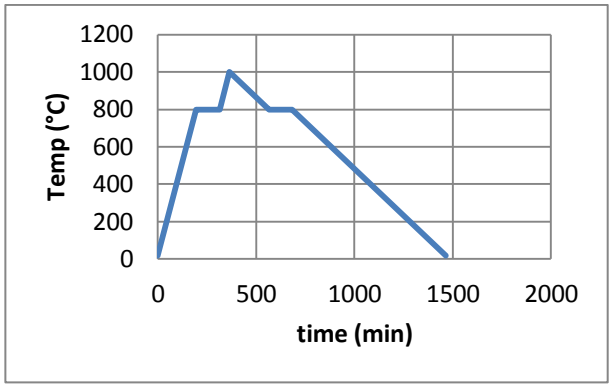


Chart 3: Temperature diagram for the 3rd series

### 4.5.4 Series 4

The fourth series of frits was made in the same way as the first set, except that the maximum temperature was 1000 °C, also as in the 3rd series with machined ground frits, we try to lower the porosity in the seal. When comparing to 3rd series we can see the influence of the isothermal steps and the influence of increased temperature, when compared to series 1.

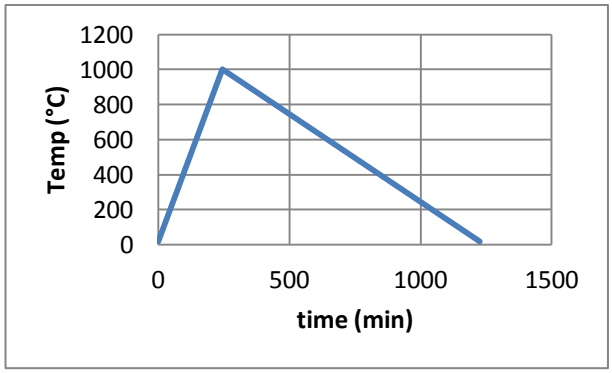


Chart 4: Temperature diagram for the 4th series

## 4.6 Crafting a feedthrough

The crucial part in manufacture of the implanted unit is the fusion of Pt wire into the ceramic housing. The frit, not only must seal the gap between the wire and the housing, it must also withstand the mechanical load that is constantly present during usage. That is why we shaped a bored hole in the housing in form of a coin (figures 28 and 29). The impact of the possible tensile strength and the torsion, which can be present between housing and the stimulator through the Pt wire, is therefore minimized much more effectively than with a straight borehole.

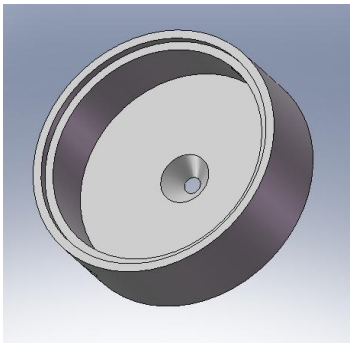

Figure 28: Ceramic housing with coin shaped borehole (model)

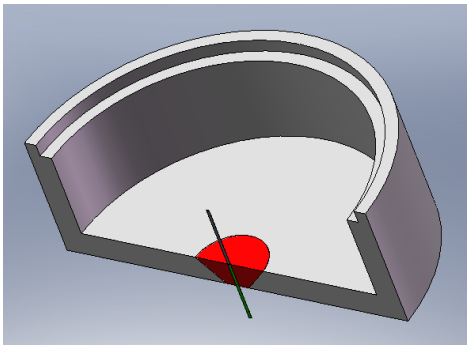

Figure 29a, b: Feedthrough formation: fused Pt wire with a frit (model)

In addition with a coin shaped hole we increase the bonding surface Macor/frit by at least 5 times which consequently strongly increases the general quality of the formed seal.

The lid and crucible were machined out of a Macor rod (standard commercial dimensions), using universal lathe machine (Litostroj Potisje, Ada, Serbia). Holes were made using custom shaped drills.

## 4.7 Feedthrough manufacturing

The procedure of frit sealing was adopted from the recommendations given by the manufacturers of the Macor ceramic and frits. The GLP steps were followed through all procedure of manufacturing [91, 92]. Those steps are described below.

### 4.7.1 Fabrication of the crucible and the lid

The crucible and the lid were fabricated using lathe machine (Litostroj Potisje, Ada, Serbia). The surface of the pieces was very fine since carbide cutting tools were used.

### 4.7.2 Drilling the holes

Same as in previous step, no special tools were needed to drill the holes in a specific shape; however, it was needed that the tool was brushed to certain geometry. For drilling the holes we used Black & Decker power drill KR753 (Stanley Black & Decker, Stanley Drive, USA).

### 4.7.3 Cleaning

Cleaning of specimens and tools was done using an ultrasonic cleaner Branson 2510 (Branson Ultrasonic corporation, Danbury, USA) with deionized water. Afterwards, the specimens were rinsed in acetone and air dried.

### 4.7.4 Drying

After ultrasound cleaning, specimens were dried at 200 °C for 2h in a universal temperature chamber Kambič SP-45C (Kambič laboratorijska oprema, Semič, Slovenia).

### 4.7.5 Frit grinding/milling

For the first two series we manually grinded the frits for 30 minutes using laboratory polished agate mortar (Wenk LabTec GmbH, Nettetal, Germany) and for the next two series the frits were ground for 1 hour in a planetary balls mill Retsch PM100 (Retsch GMBH, Haan, Germany) using YSZ balls.

### 4.7.6 Frit drying

Frits were dried before use at 200 °C for 2h in an universal temperature chamber Kambič SP-45C.

### 4.7.7 Preparing pins

The pins were made from 10 mm long Pt wire of 0,3 mm diameter. Pins were formed to a shape of a letter L to be more stable during embedding of the frits. All feedthroughs for individual series were made on the same piece of Macor ceramic at the same time (figures 36, 37, 44 and 45). Crucible of Macor ceramic was positioned on the working table in a way that a tops of coin shaped holes were facing down (figures 28, 29, 36 and 44). The pins were inserted in the holes in the same position as is the letter L.

### 4.7.8 Frit embedding

Individual frits were inserted in a holes using small laboratory stainless steel spatula. Moderate pressure with hand was used for embedding the frits around pins. The quantities of frits were such that formed surfaces on top were even with a Macor crucible surface. The procedure was also the same for all three steps within the second series.

We didn't use any fixture for the pins (geometry issue). Consequently we repeated embedding for a few times because of undesirable shift of Macor crucible resulted in movement of the pins and decay of embedded frits. The procedure was time consuming.

### 4.7.9 Frit sealing

Four series of feedthroughs were made. For all series the maximum temperature of sealing was 1000 °C (except for 1$^{st}$ series 900 °C) with a heating rate of 4 °C/minute and a cooling rate of 1 °C/minute in a Protherm laboratory furnace PLF 100/3 with oxidative atmosphere.

### 4.7.10 Repeating the sealing cycles

The sealing of the frits within second series was repeated two times. Each time one side of the sealed surfaces was additionally covered with frits in order to fulfill the complete volume of forming feedthrough.

### 4.7.11 Surface sealing

The first series of feedthroughs had an additional procedure to achieve better surface sealing and to decrease permeability (decreasing the likelihood of leakage of inner body fluids inside the implanted unit). On the outer side of the crucible we deposited pure Pt using thermal evaporation in a Balzers vacuum chamber (Pfeiffer Vacuum, Asslar, Germany). An oil rotary turbo pump Balzers Pfeiffer duo 1,5A (Pfeiffer Vacuum, Asslar, Germany) achieved a vacuum of $10^{-6}$ bar. During evaporation the pressure was slightly decreased. The thickness of a layer was about 150 nm. On the inner side we evaporated pure Ti using a Thermionics 3 kW research capacity series single crucible e-Gun (Thermionics laboratory, Inc, Hayward, USA). Again a vacuum of $10^{-6}$ bar was achieved by Edwards oil-free rotary turbo pump (Edwards, Crawley, United Kingdom). The thickness of a Ti layer was 650 nm with a forming speed of 8 Å/s.

### 4.7.12 Annealing

To release stresses in the samples after the above procedures, we annealed the samples using heating and cooling rates of 3 °C/h at a temperature of 700 °C for 15 minutes. Same furnace was used as for sealing the frits.

# 5 Methods and results

## 5.1 XRD analysis

XRD analysis of Macor and frits were done on a Panalytical X`pert PRO MPD device equipped with empyrean tube Cu LFF, PW 3064/60 (Reflection-Transmission Spinner), theta/theta goniometer PW3050/60 and X`Celerator detector (Panalytical B.V., Almelo, The Netherlands).

Measuring conditions were:

- start angle: 5 °
- end angle: 90 °
- steps size: 0,0167:

Pattern analysis was performed with Panalytical software X'Pert HighScore version 2.1.b.

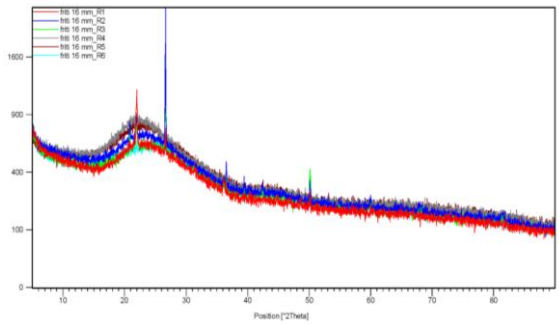

Figure 30: XRD analysis of frits –2D comparison chart

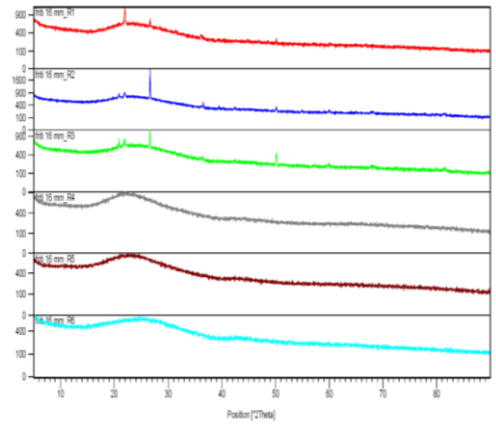

Figure 31: Roentgenograms for individual frits

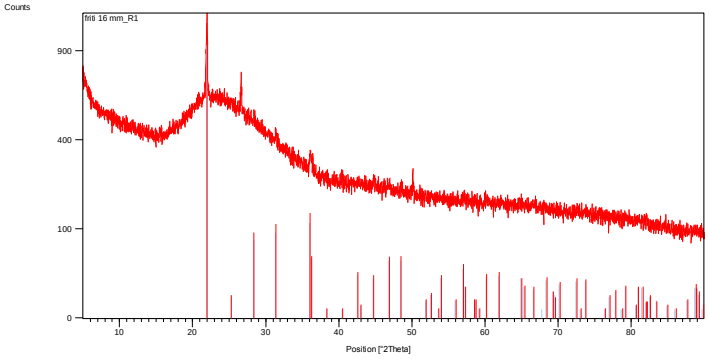


| Visible | Ref. Code | Score | Compound Name | Displacement (°2Th.) | Scale Factor | Chemical Formula |
|---|---|---|---|---|---|---|
| * | 01-071-0785 | 30 | Cristobalite | 0,000 | 0,923 | Si O2 |

Figure 32: Pattern of frit R1 and matching $SiO_2$ characteristic peaks

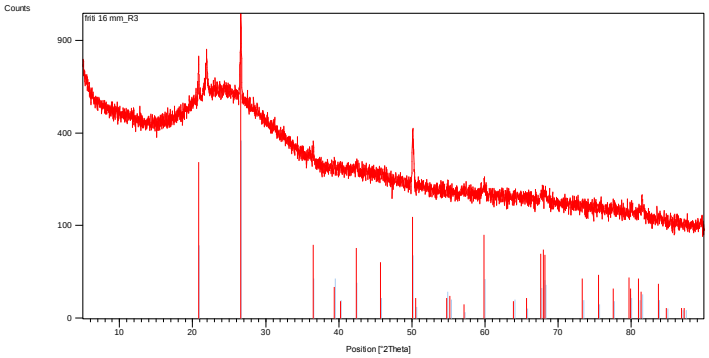


| Visible | Ref. Code | Score | Compound Name | Displacement (°2Th.) | Scale Factor | Chemical Formula |
|---|---|---|---|---|---|---|
| * | 01-089-1961 | 40 | Quartz | 0,000 | 1,049 | Si O2 |

Figure 33: Pattern of frit R3 and matching $SiO_2$ characteristic peaks

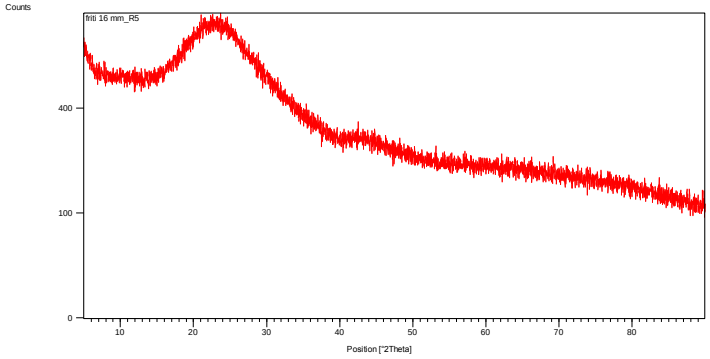


Figure 34: Pattern of frit R5 with 100 % of glassy microstructure

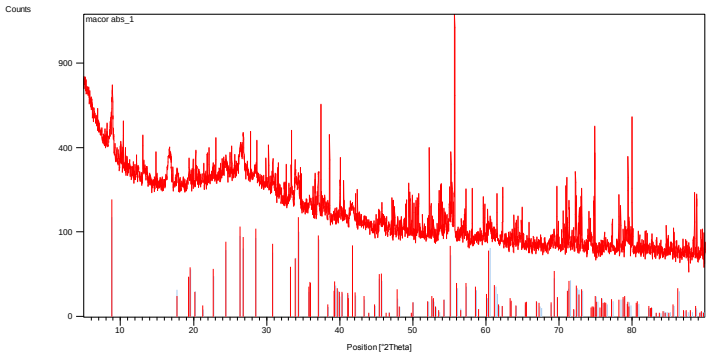


| Visible | Ref. Code | Score | Compound Name | Displacement (°2Th.) | Scale Factor | Chemical Formula |
|---|---|---|---|---|---|---|
| * | 01-071-1542 | 20 | Fluorphlogopite 1\ITM\RG, syn | 0,000 | 0,128 | K Mg3 Al Si3 O10 F2 |

Figure 35: Pattern of Macor and matching Fluorphlogopite characteristic peaks

### 5.1.1 Results of XRD analysis

XRD identification is possible, when material is in crystalline state. Roentgenograms of frits (figure 30 to 34) display only a few characteristic peaks if any at all - which is typical for glassy materials. Roentgenogram of Macor ceramic (figure 35) is showing crystalline microstructure constituent Fluorphlogopite Mica.

## 5.2 Microscopy

Microscopy was done using laboratory microscope Nikon Eclipse E20 (Nikon Corporation, Tokyo, Japan) with magnifications 40x and 100x fitted with a Lumenera camera Infinity 1 and Infinity Capture and Analyze software (Lumenera Corporation, Ottawa, Canada).

Embedding of materialographic specimens was made using cold mounting acrylic resin with mineral filler. Specimens were brushed and polish with Struers labopol-1 (Struers A/S, Copenhagen, Denmark). The feedthroughs were labeled according to individual series and frits (table 10).

Table 10: Labeling the feedthroughs

| feedthrough series | frit 1 (R1) | frit 2 (R2) | frit 3 (R3) | frit 4 (R4) | frit 5 (R5) | frit 6 (R6) |
|---|---|---|---|---|---|---|
| 1st (S1) | R1-S1 | R2-S1 | R3-S1 | R4-S1 | R5-S1 | R6-S1 |
| 2nd (S2) | R1-S2 | R2-S2 | R3-S2 | R4-S2 | R5-S2 | R6-S2 |
| 3rd (S3) | R1-S3 | R2-S3 | R3-S3 | R4-S3 | R5-S3 | R6-S3 |
| 4th (S4) | R1-S4 | R2-S4 | R3-S4 | R4-S4 | R5-S4 | R6-S4 |

### 5.2.1 Series 1: 900 °C

For the first series we fused 6 frits at a temperature of 900 °C (figures 36 and 37).

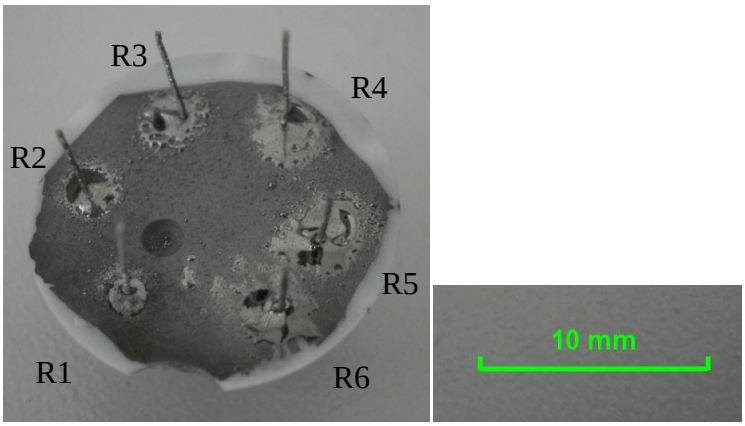


Figure 36: Inner surface of crucible with Ti coating (series 1, 900 °C)

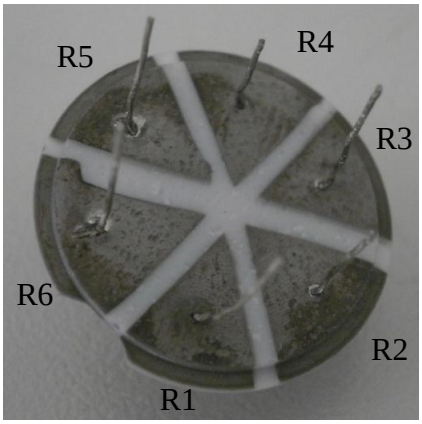


Figure 37: Outer surface of crucible with Pt coating (series 1, 900 °C)

Below are shown the microstructures (40x magnification).

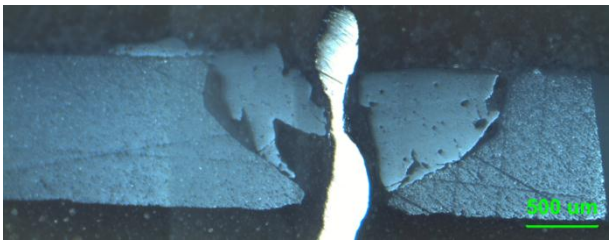

Figure 38: Feedthrough R1-S1

Among this series the seal R1-S1 (figure 38) was not bonded with Macor and Pt. The reason was the chemical composition of the frit and thus the higher melting temperature of frit R1.

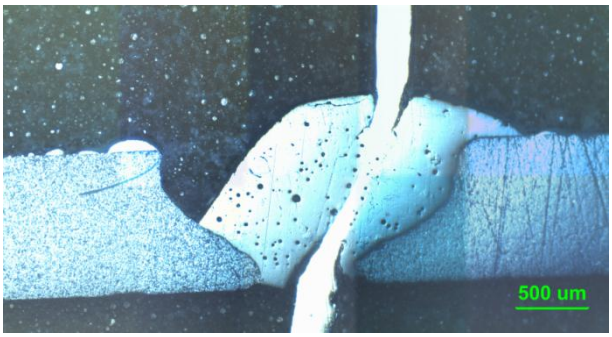


Figure 39: Feedthrough R2-S1

In figure 39 is the cross-section of the formed seal R2-S1. The interphase between Macor and frit is clearly shown. The seal did not form an interphase on whole surface of the Macor. This result was expected since Macor is known as having a non-wetting surface. The frit is showing evenly dispersed porosity; air holes are mostly of same size and also dispersed along the Pt wire. Wetting of the Macor ceramic is not ideally, while the wetting of the Pt wire is good. Wetting angle is high.

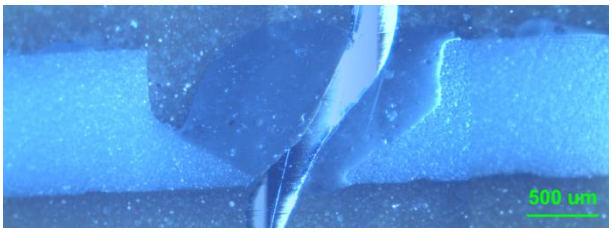


Figure 40: Feedthrough R3-S1

Seal R3-S1 (figure 40) is very similar to R2-S1 since the chemical composition is similar. In general we can say that wetting of Macor surface was better when Pt wire was close to it for all frits (capillary effect). Wetting is similar as in case of seal R2-S1.

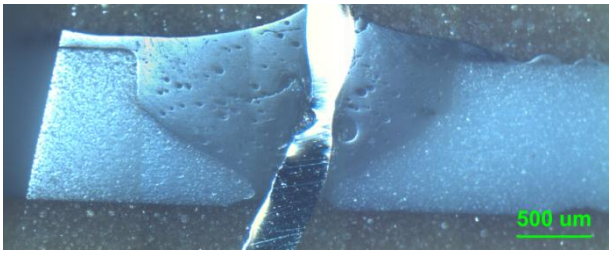


Figure 41: Feedthrough R4-S1

Frit R4 (figure 41) gave the highest wettability of Macor within selected frits. The porosity is not high, it is unevenly dispersed, but the air holes are larger along Pt wire. Wetting of Macor and Pt is perfect.

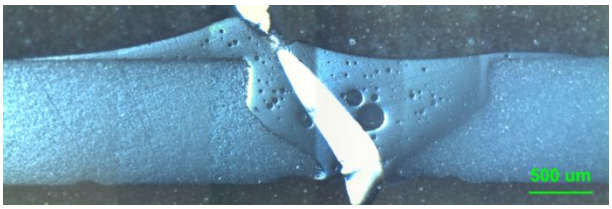


Figure 42: Feedthrough R5-S1

Another frit (figure 42) with good wettability of Macor ceramic is frit R5. Air holes are not finely distributed, especially along Pt wire where the holes are bigger with diameter of up to 0.17 mm. Same as frit R4, frit R5 perfectly wets Macor and Pt.

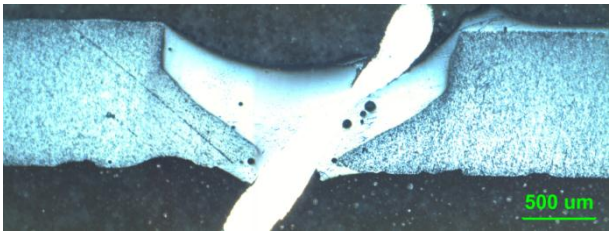


Figure 43: Feedthrough R6-S1

R6-S1 seal (figure 43) has very low porosity; some holes are present along Pt wire. Wetting of Macor and Pt wire is not optimal and seal did not fulfill hole. The wetting is not optimal, although better than in case of frits R2 and R3.

#### 5.2.1.1 Results of the series 1

The technical approach used for the 1st series turns out to be successful on a microscopic level. Regarding wetting, the best results were achieved with frits R4 and R5 where the hole was completely filled. Frit R6 also wetted surface of the hole, but it was not enough for the whole hole to be filled. Partially wetted surface of Macor was achieved by frits R2 and R3. Frit R1 did not form a seal.
The wetting angles among frits are different. Frits R4 and R5 perfectly wets Macor ceramic and Pt wire.

### 5.2.2 Series 2: 1000 °C

For the second series we fused 6 frits at a maximum temperature of 1000 °C (chart 2, figures 44 and 45) the cycle was repeated three times. By doing so, we can determine the influence of raising the temperature and also whether this procedure provides better wettability, lower porosity and better filling of the gap between the Pt wire and crucible. Frit R1 also under this procedure did not fuse Pt wire with Macor.

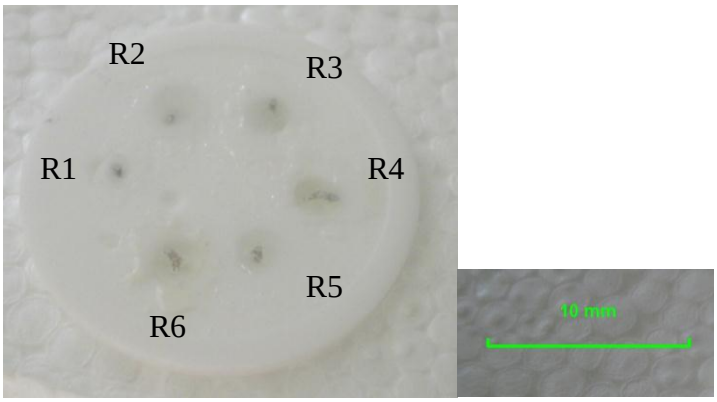


Figure 44: Inner surface of crucible (series 2, 1000 °C)

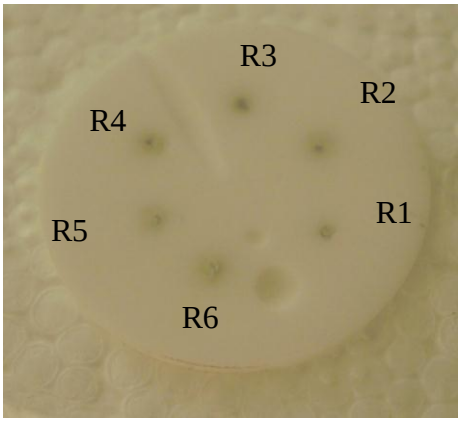


Figure 45: Outer surface of crucible (series 2, 1000 °C)

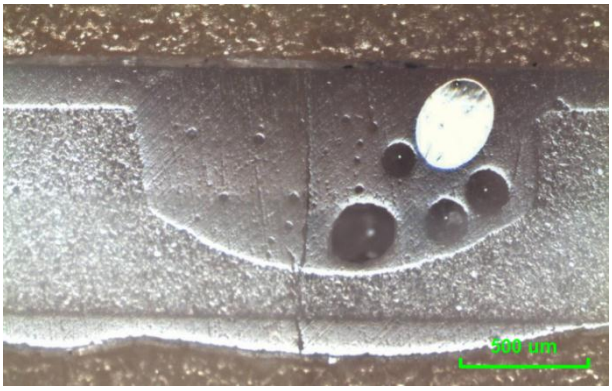


Figure 46: Feedthrough R2-S2

The seal formed in R2-S2 (figure 46) perfectly fills the hole. Seal shows minor porosity opposite to the Pt wire, while there are large air inclusions around the Pt wire.

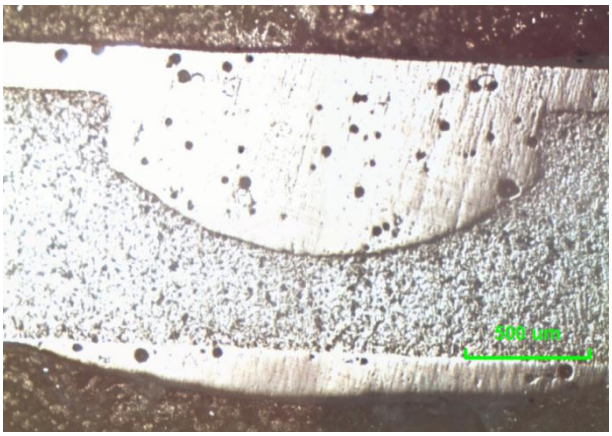


Figure 47: Feedthrough R3-S2

Frit R3 (figure 47) behaves in a similar ways to R2 and fully seals the hole. The porosity is evenly dispersed.

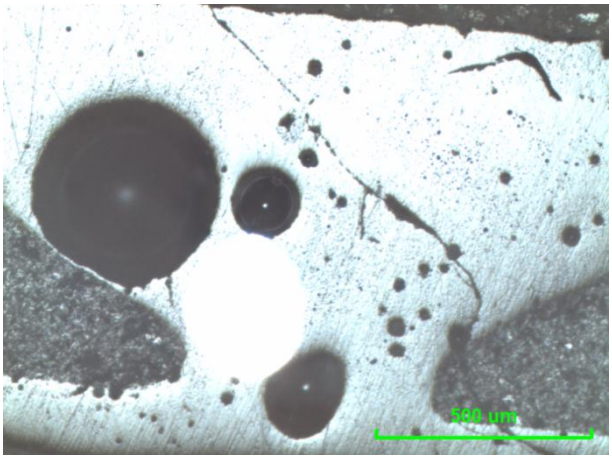


Figure 48: Feedthrough R4-S2

Although perfectly, the wetted seal R4-S2 (figure 48) contains large air inclusions. When forming seal, inclusions are moving toward Pt wire and eventually they surround wire.

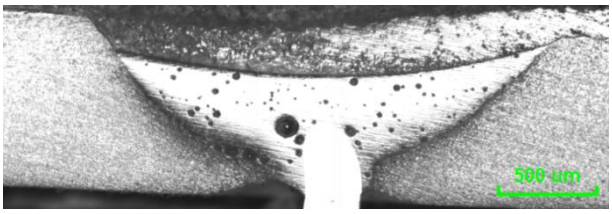


Figure 49: Feedthrough R5-S2

The sealing of frit R5 (figure 49) was repeated separately one more time and undergone only one cycle. This is the reason why hole is not fully filled. Porosity is present and finely dispersed.

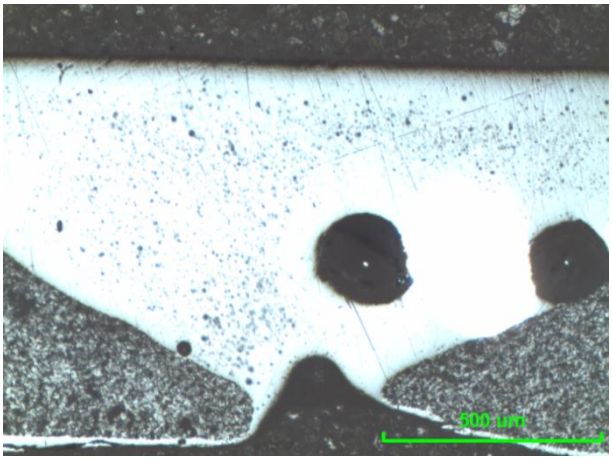

Figure 50: Feedthrough R6-S2

In figure 54 are two large air inclusions surrounded by area with no porosity. This confirms in thermodynamic known phenomena to decrease surface energy: small inclusions are grouping together to form large ones. Certain diffusion and temperature conditions for that matter must be accomplished. The rest of seal R6-S2 exhibit fine dispersed porosity.

#### 5.2.2.1 Results of the series 2

In the second series the porosity is very finely dispersed, but along the Pt wire we see very large air inclusions. It is evident that small inclusions are grouping together and form large ones in presence of thermally more conductive metal (Pt wire). Thermodynamically is this the preferred situation.
Higher sealing temperature is reflected also in better wetting of the Macor ceramic. In general all frits optimal wetted Macor surface

### 5.2.3 Series 3: 1000 °C


Figure 51: Feedthrough R2-S3

Partially wetting and high porosity of seal R2-S3 is shown in figure 51.

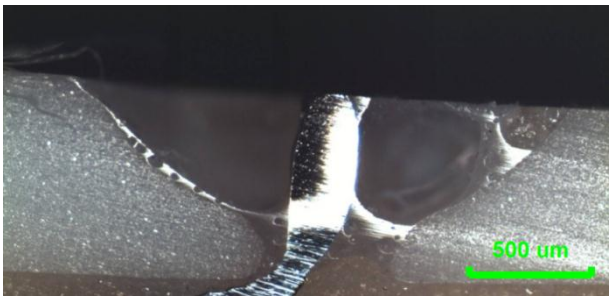


Figure 52: Feedthrough R3-S3

The wetting of Macor ceramic is perfect (figure 52), but perfect seal with frit R3 is not formed. Sample R3 is having largest porosity among this series.

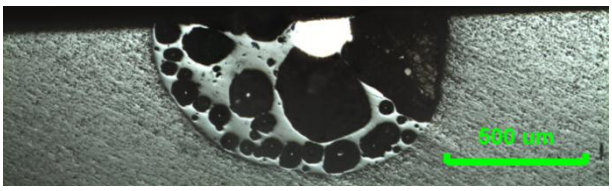


Figure 53: Feedthrough R4-S3

Better, but still inadequate formed seal R4-S3 with high porosity (figure 53).

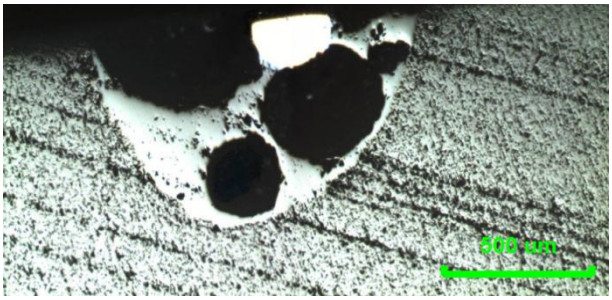


Figure 54: Feedthrough R5-S3

Formation of seal R5-S3 is similar to feedthrough R4-S3 (figure 54) in 2nd series same frits (R4 and R5) formed perfect seal.

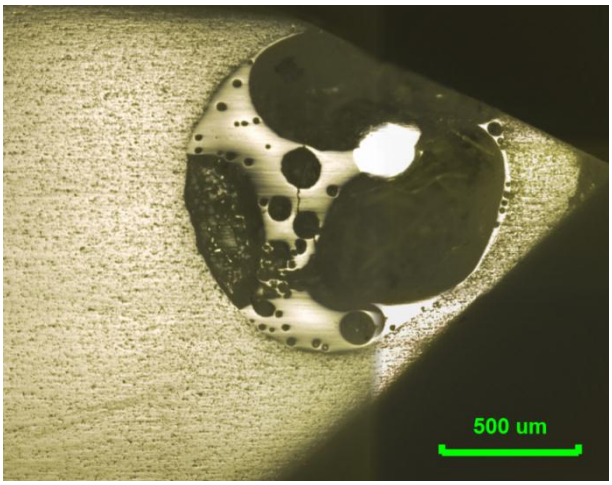


Figure 55: Feedthrough R6-S3

Wetting of Macor ceramic is not problematic for the 3rd series. High porosity appears in all seals, also when using frit R6 (figure 55).

#### 5.2.3.1 Results of the series 3

Results for this series were completely unexpected. Frits were milled in the machine for the third series. Uniform size of that way prepared particles affecting the green density of embedded frits which is lower and exhibit more porosity. At microscopic level of sealed feedthroughs we can't observe fine dispersed porosity as in previous series. Air inclusions are rather large and less of hole is fulfilled with a frit. It is

possible that this effect is because of introduced isothermal steps. Seams that machined milled frits provide better results regarding elimination of fine dispersed porosity, although one cycle per series is not enough to completely seal the area.
Wetting of the Macor ceramic is more similar to the 1st series than the 2nd. Wetting of the Macor surface is better near Pt wire.

### 5.2.4 Series 4: 1000 °C

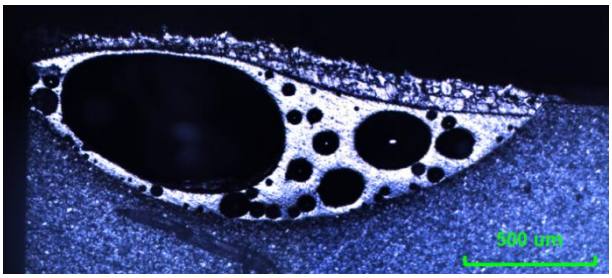


Figure 56: Feedthrough R2-S4

Frit R2 completely formed a seal (figure 56) but the porosity is very high. Frit fully wetted the Macor surface.

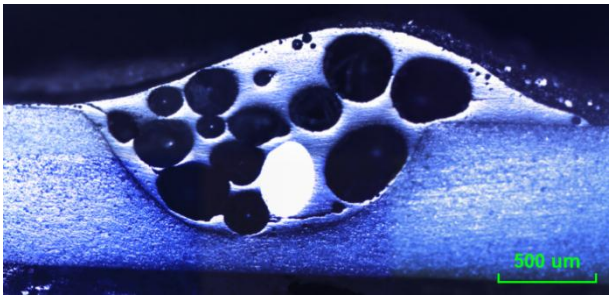


Figure 57: Feedthrough R3-S4

Seal R3-S4 (figure 57) is better than that of series S3 although the porosity is higher than expected. Complete Macor surface is wetted.


Figure 58: Feedthrough R4-S4

Seal R4-S4 (figure 58) was formed across the interphase of the Macor/frit. Air inclusions are bigger and uneven size. Porosity is forming near Pt wire. Wetting of the Macor surface is good.

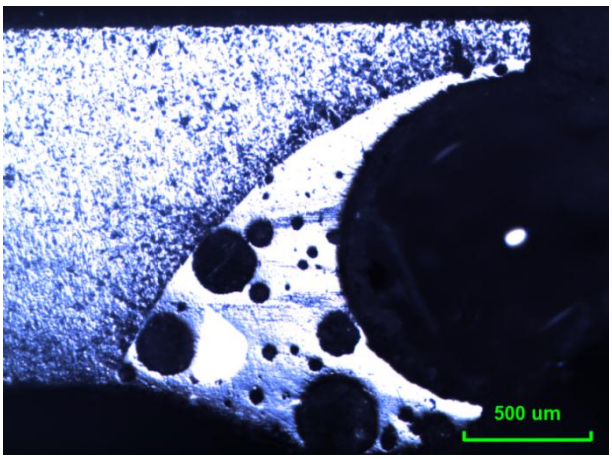


Figure 59: Feedthrough R5-S4

The porosity in seal R5-S4 (figure 59) is also high as seen in earlier frits in this series. Compared to seal R3-S4, air holes are of various sizes.

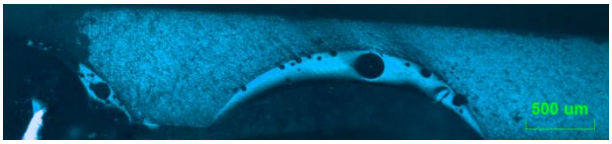


Figure 60: Feedthrough R6-S4

Frit R6 (figure 60) forms a seal only along Macor/frit interphase. Seal formation is similar to that of the same frit at the first series. The whole Macor surface formed bond with frit.

#### 5.2.4.1 Results of the series 4

Analysis of the 4$^{th}$ series shows that there are similar formed seals than in the 3$^{rd}$ series but not as good as in the second series. To completely form a seal, same procedure as for the second series should be introduced.

Regarding optical microscopy, wetting achieved at 4$^{th}$ series is better than that of the 3$^{rd}$.

## 5.3 SEM/EDX analyses

SEM analysis was made on feedthrough R6 of first and second series and EDX analysis on sample R6 of first series using following equipment (Carl Zeiss Microscopy, Peabody, USA):

- Carl Zeiss SMT SUPRA™ 40 Field Emission Scanning Electron Microscope
- GEMINI EFSEM (electron beam generation)
- EDAX x-ray analyzer

The EHT parameter of SEM analysis was 3.00 kV. Even at these lower voltages there was a problem with charging reflected in limited magnification and white spots on figures.

### 5.3.1 SEM analysis of feedthrough R6-S1

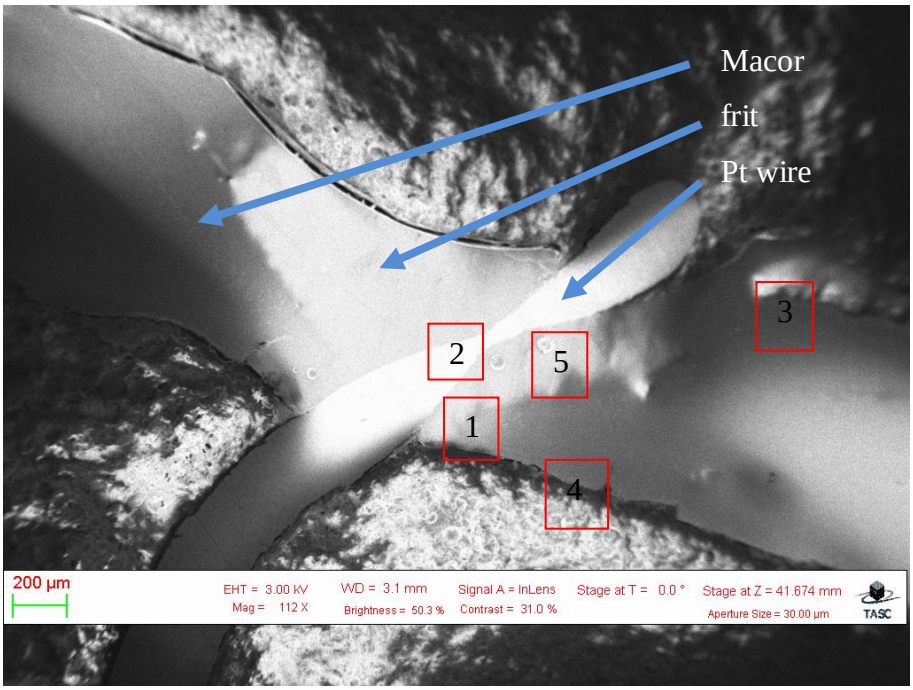


Figure 61: Feedthrough R6-S1with marked positions of SEM analyses

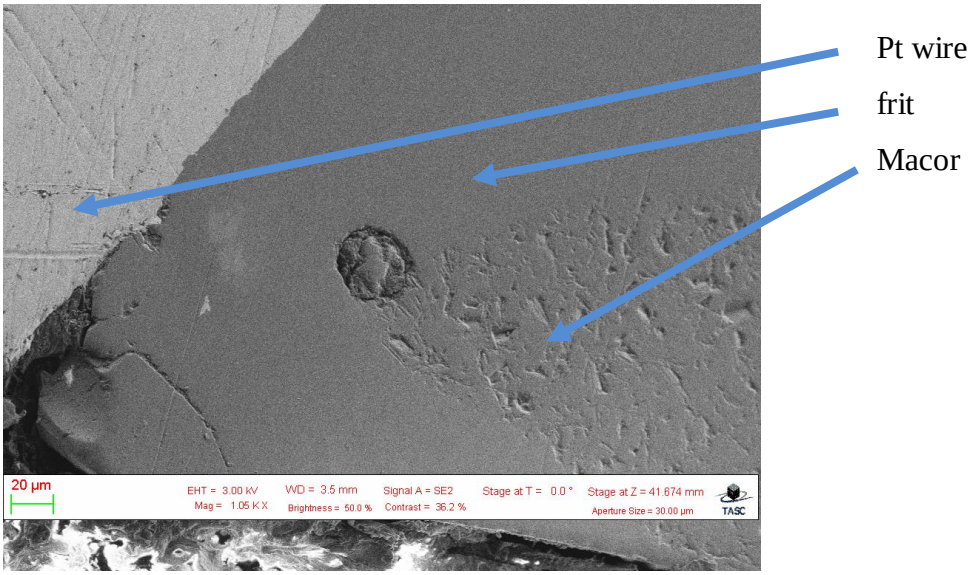


Figure 62: SEM analysis of position 1 (magnification 1050 x)

10

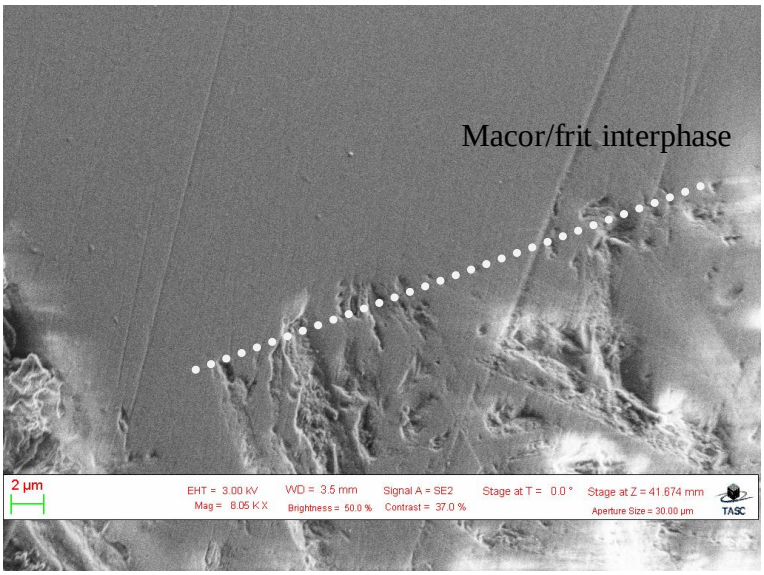


Figure 63: SEM analysis of position 1 (magnification 8050 x) with indicated Macor/frit interphase

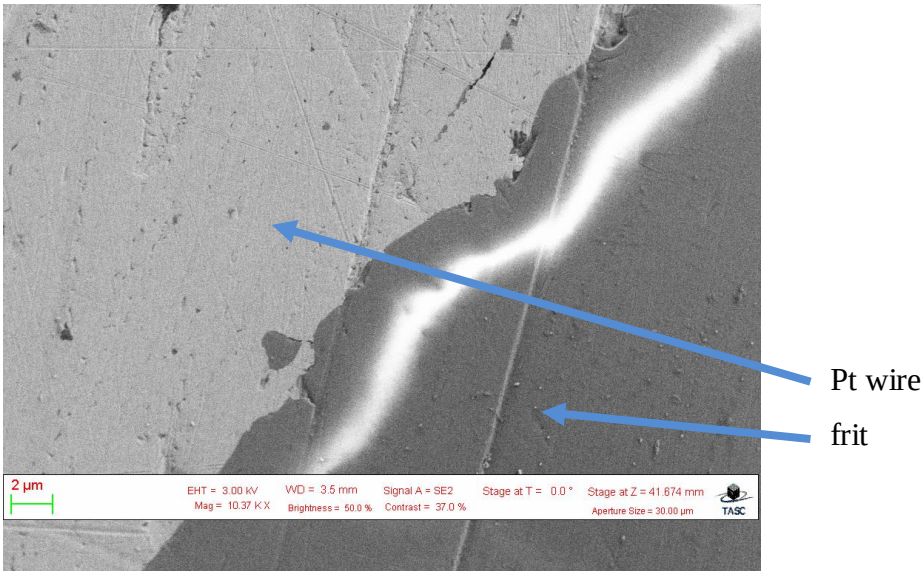


Figure 64: SEM analysis of position 2 (magnification 10370 x) on interphase Pt wire/frit

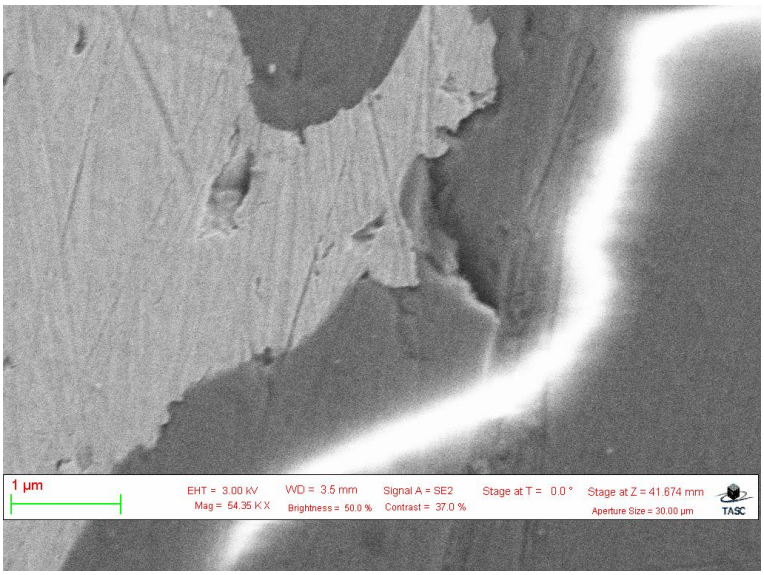


Figure 65: SEM analysis of position 2 (magnification 54350 x)

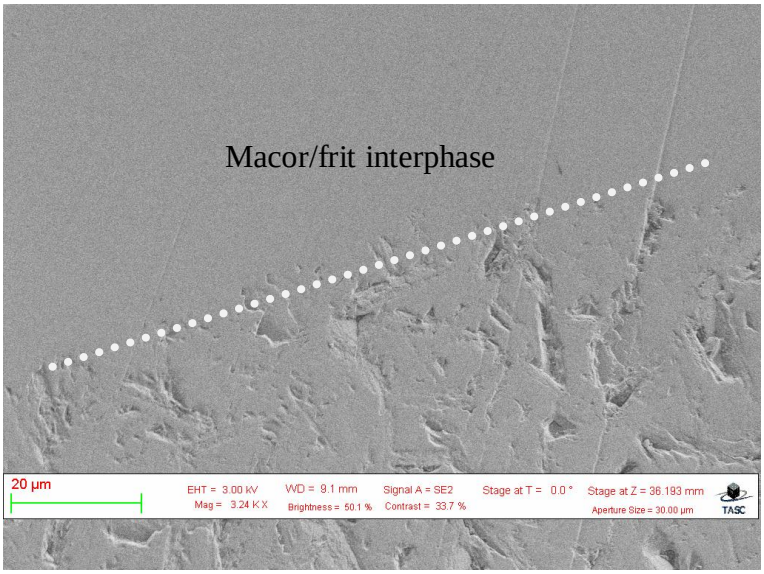


Figure 66: SEM analysis of position 3 (magnification 3240 x) on interphase Macor/frit

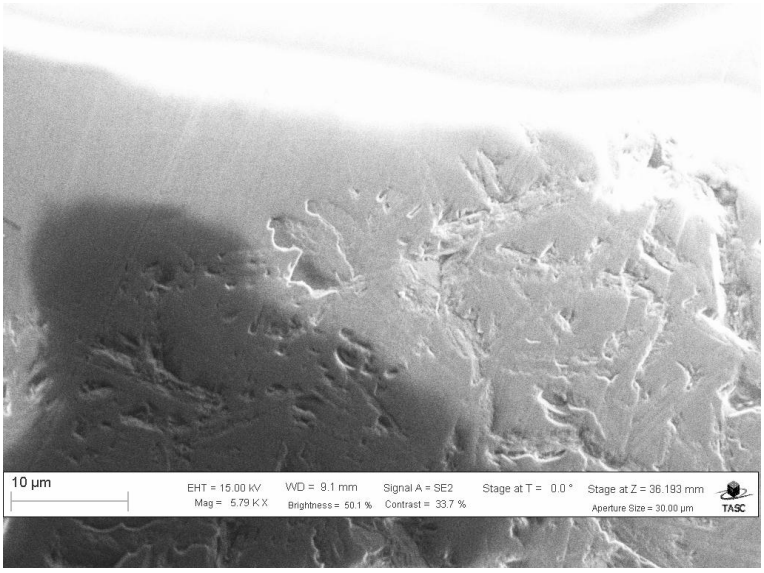


Figure 67: SEM analysis of position 3 (magnification 5790 x)

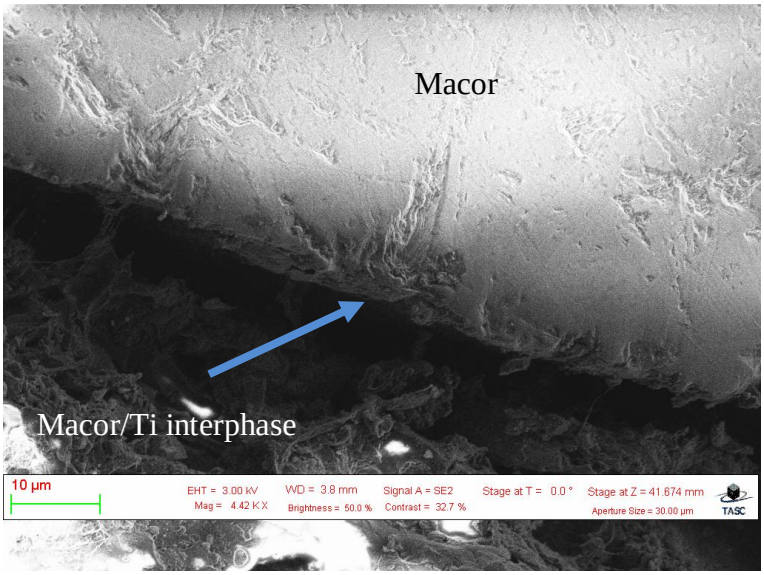


Figure 68: SEM analysis of position 4 (magnification 4420 x) on interface Macor/Ti

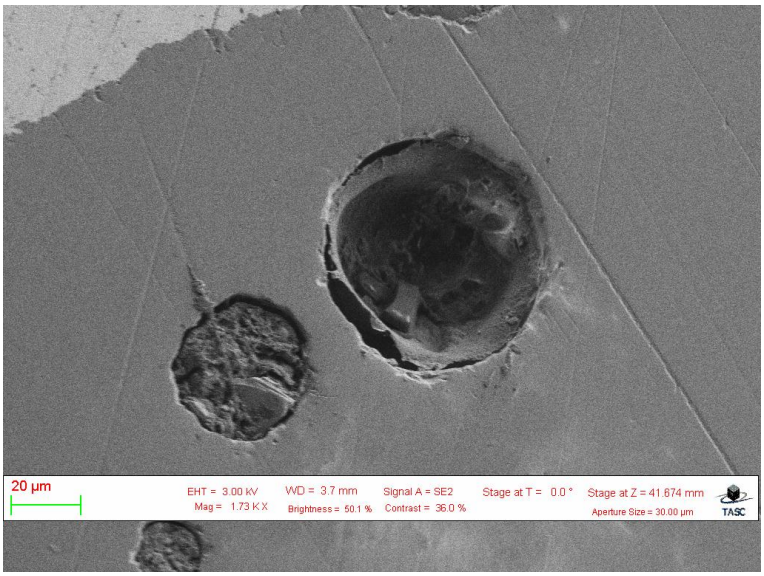


Figure 69: SEM analysis of position 5 (magnification 1730 x) with air inclusions

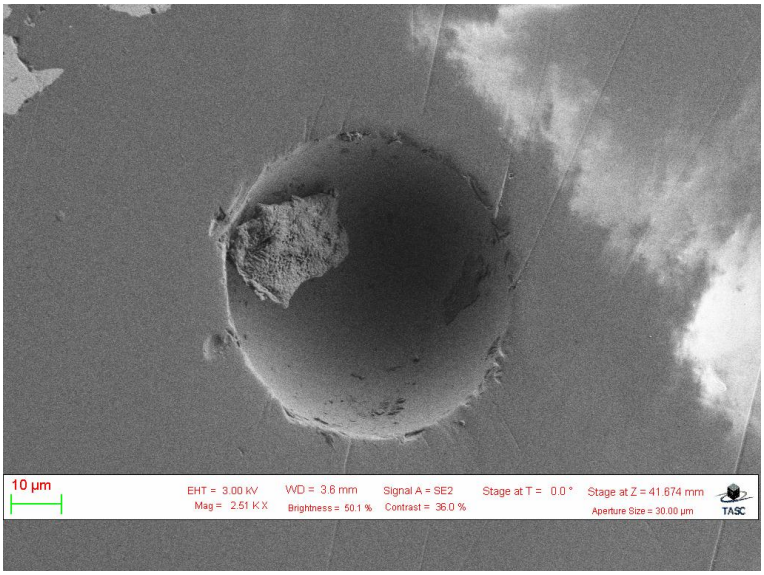


Figure 70: SEM analysis of position 5 (magnification 2510 x)

#### 5.3.1.1 Results of SEM analysis of sample R6-S1

In figures 61 to 70, the frit is the darker smooth phase, Macor darker rough and the Pt light phase.

Figures 64 and 65 show a perfectly wetted Pt wire. There are irregularities along border but they do not exceed 1 µm.

While the Macor crystal phase doesn't changed during the fusion procedure, the glassy phase of the borosilicate glass perfectly remelts with the frit (figure 66). Even at higher magnifications (figure 67) there is no evidence of any irregularities in the new interphase.

In figure 68 the layer of Ti is shown, due to problems at higher magnifications it is difficult to see. As the roughness of the surface exceeds 1 µm and because the sputtered layer of Ti is just above 0.5 µm, a uniform thin layer of Ti cannot be formed. To do that the surface would have to be polished and/or the thickness of the sputtered film increased.

Porosity is important. Formed air inclusions are in different sizes up to 50 µm (figures 69 and 70). Air inclusions can be in shape of a perfect sphere (figure 70) and can carry different phases (figure 69) as a result of kinetics.

### 5.3.2 SEM analysis of feedthrough R6-S2

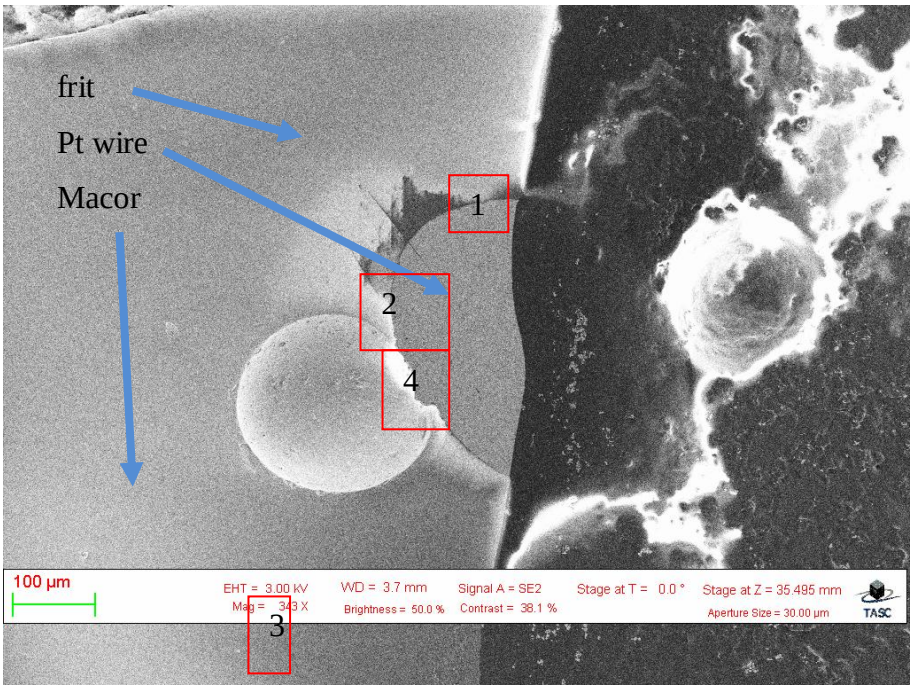


Figure 71: SEM analysis of feedthrough R6-S2 (magnification 343 x)

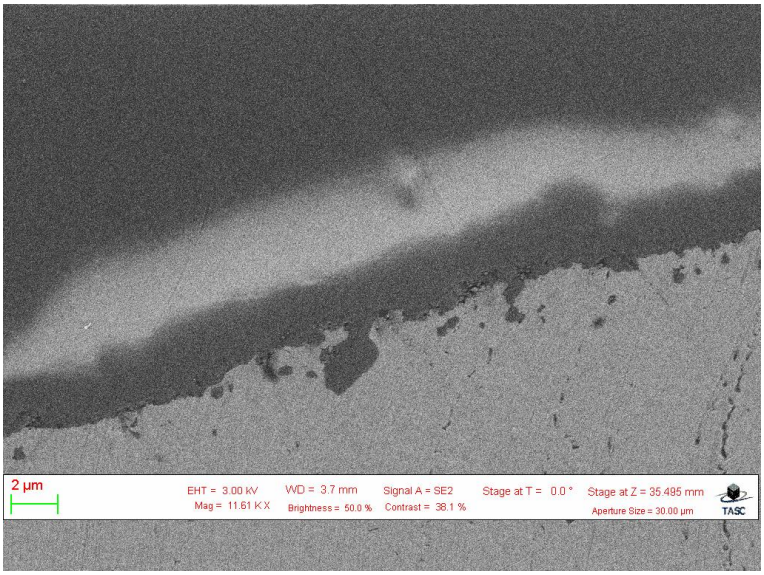


Figure 72: SEM analysis of position 1 (magnification 11610 x) on interface Pt wire/frit

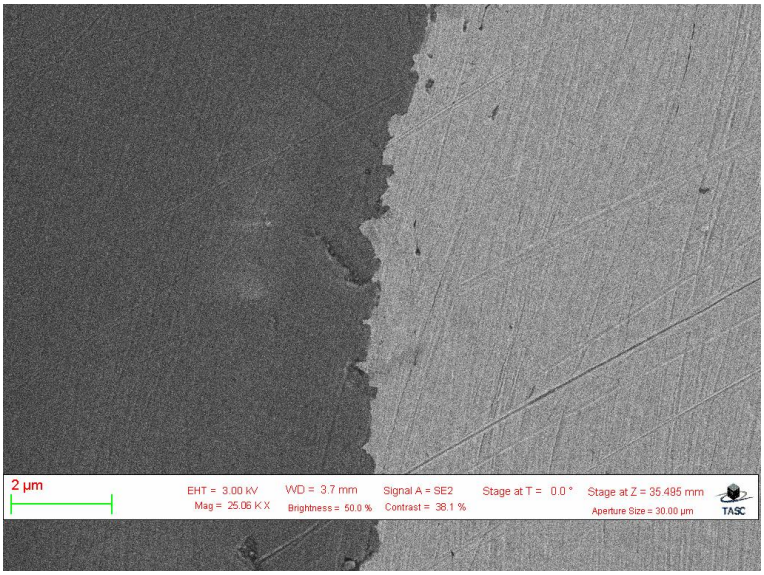


Figure 73: SEM of position 2 (magnification 25060 x) on interface Pt wire/frit

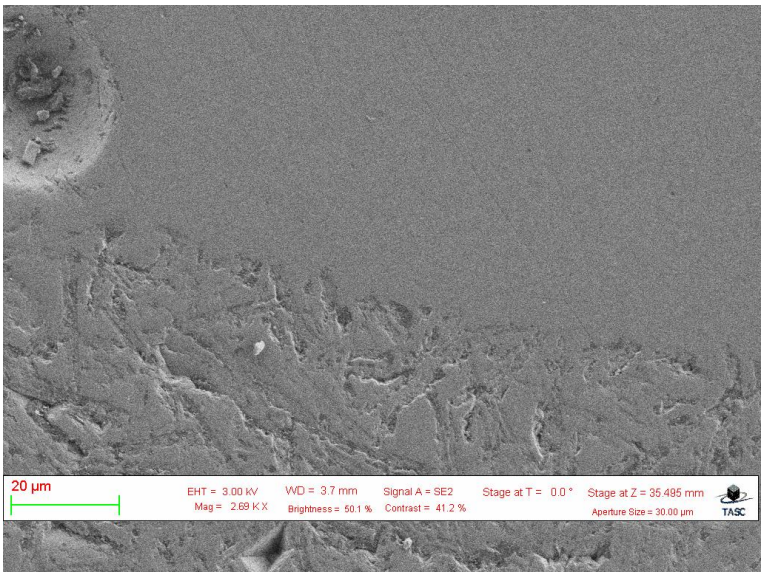


Figure 74: SEM of position 3 (magnification 2690 x) on interface Macor/frit

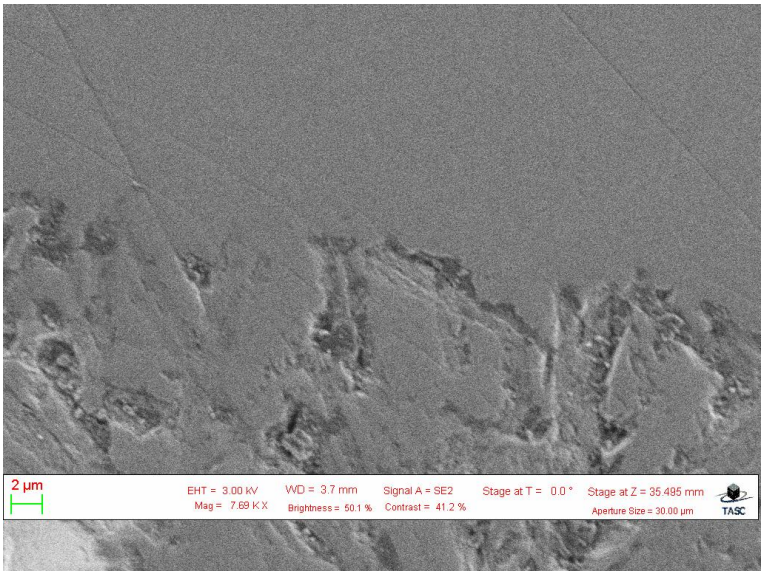


Figure 75: SEM of position 3 (magnification 7690 x)

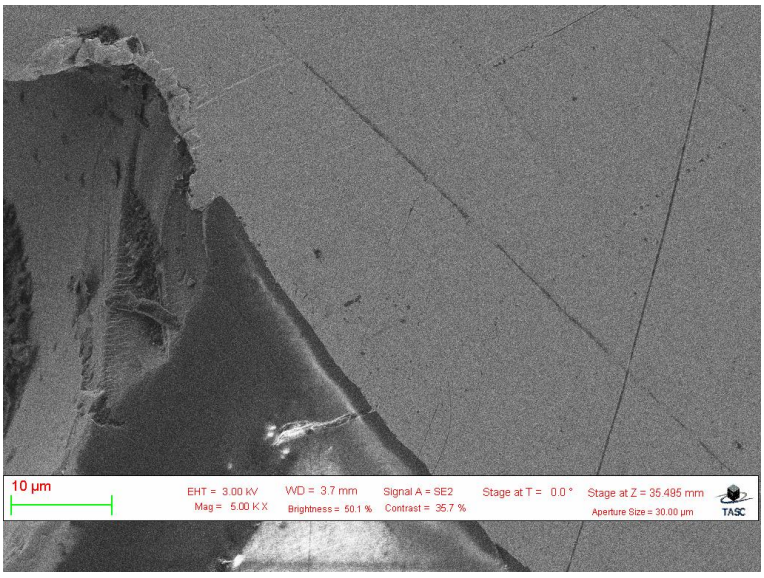


Figure 76: SEM of position 4 (magnification 5000 x) on the edge of air inclusion

#### 5.3.2.1 Results of SEM analysis of sample R6-S2

SEM analysis of the 2nd series of feedthroughs (figures 71 to 76) gives us a similar but not identical picture as the first.

The wetting of the Pt wire (figures 72 and 73) is perfect. There are irregularities along border also not exceeding 1 µm which is expected since fusion took place at higher temperatures and was repeated 3 times.

At the interphase of the Macor/frit (figures 74 and 75) it can be seen that crystal phase changes along the phase border. Still the border between the Macor/frit is clear and the borosilicate phase of Macor is well incorporated to frit microstructure.
The kinetics of porosity formation is also different. It seems that small air inclusions have combined and formed large ones around Pt wire (figure 76) since the Pt is more thermal conductive than Macor ceramic. Diameter of the inclusions exceeds 100 μm.

### 5.3.3 EDX analysis of feedthrough R6-S1

EDX analysis was carried out on sample R6-S1on 4 positions (figure 81) starting on the frit along by regions close to interface and ending up on the Macor surface.

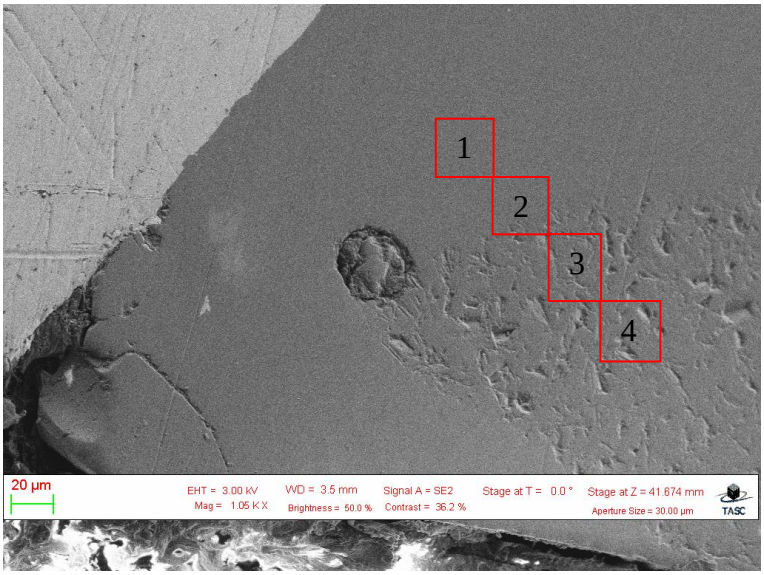


Figure 77: Positions of EDX analysis (spot 1 of SEM analysis)

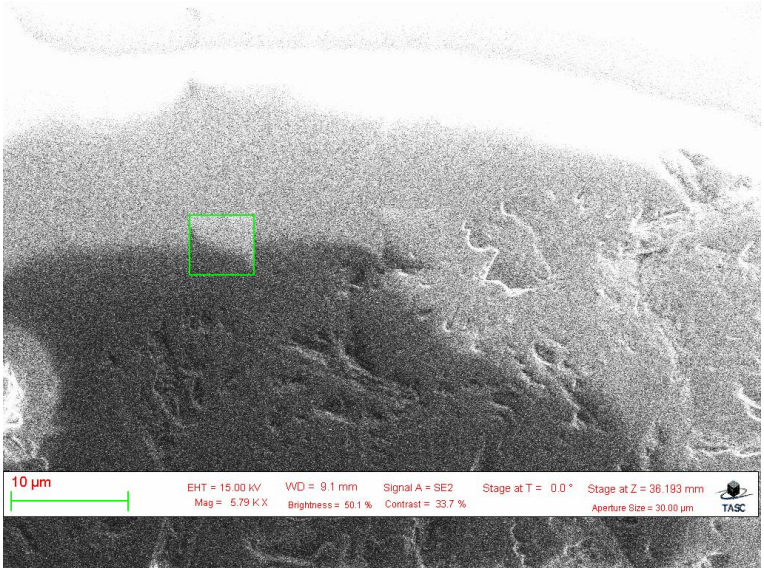


Figure 78: EDX analysis of position 2 (magnification 5790 x)

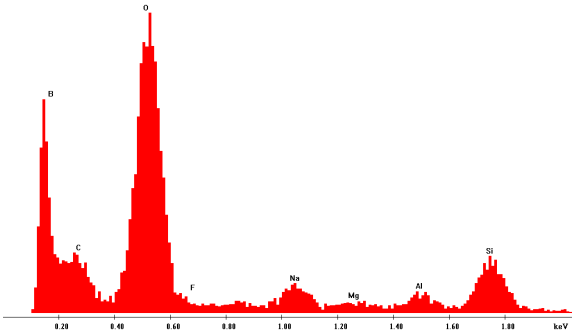


Figure 79: EDX analysis of position 1

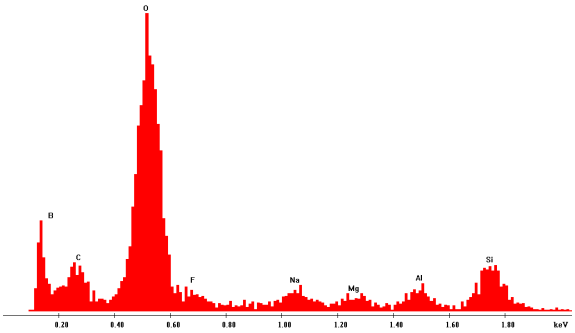


Figure 80: EDX analysis of position 2

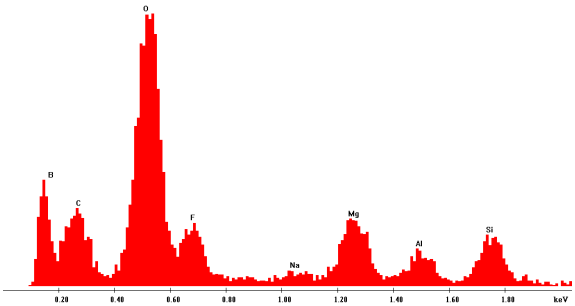


Figure 81: EDX analysis of position 3

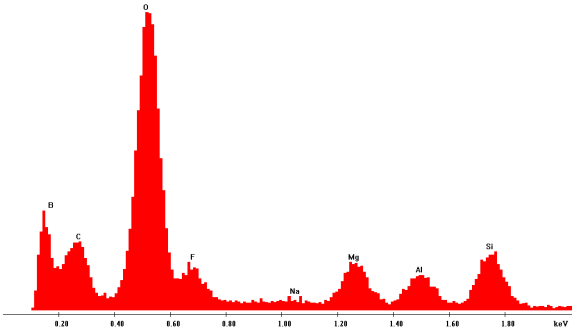


Figure 82: EDX analysis of position 4

#### 5.3.3.1 Results of EDX analysis of sample R6-S1

Each analysis covered around 50 $\mu m^2$ (figures 77 and 78). EDX analysis (figures 79-82) show that elemental composition is changing across the interphase; Mg can be found not only in the Macor but can be found also at least 20 μm from border, Si is evenly distributed, while Al and F shares are slightly higher in Macor, Na is originally only in the frit where the share of B is also higher. The interphase shows an increase in Mg, Al, F and B over the surrounding areas, leaving Na and Si seemingly not involved in this element reorganization.

# Discussion

The fusion of platinum wire into the ceramic body of implantable stimulator is very important but still a minor part in the manufacture of gait corrector.

In this pilot series we made one sample for each frit/series combination. If the sample size is very small it is hard to justify a final conclusion. In our case, the similarity between individual series can partially replace deficiency of small sample size. With each frit we made four feedthroughs. Despite different temperature programs and milling of the frits, thermodynamically, conditions were comparable. Important question that arose was about frit parts sizes and shapes, between hand grinding and machine milling. Microstructure analysis can be at this point deceiving.

We expect that the answer will be only partially known with more manufactured samples per each combination. Fully disclosure will be with introduction of vacuum step within fusion procedure.

The upper temperature limit was set at 1000 °C. At higher temperatures, microstructure of Macor ceramic would deteriorate. On the other side, achieved quality of the seal could be better at higher temperatures.

Borosilicate glass is very often used for this kind of applications [26, 28]. With slightly different chemical compositions we tried primarily to see the effect on Macor ceramic/frit interphase formation on durability of the feedthrough. It is expected, that with higher mechanical properties, less tensions are generated within the fused seal. That way it is lower possibility that the internal stresses and microstructure defects will cause potential route for leakage.

Organogram on figure 83 is presenting organization of the work. Some of work is not included in thesis like preliminary test fusions and laser welding. Laser welding is very promising technology also in the field of medical applications [38]. It delivers high energy at very narrow surface which is ideally when are temperature sensitive material or parts (electronics) nearby. We perform tests with Nd:YAG laser LVN 100 (Inlaser, d.o.o., Ljubljana, Slovenia) at manufacturer company. For optimal results proper parameters (power, time) and shape of welding materials must be met.

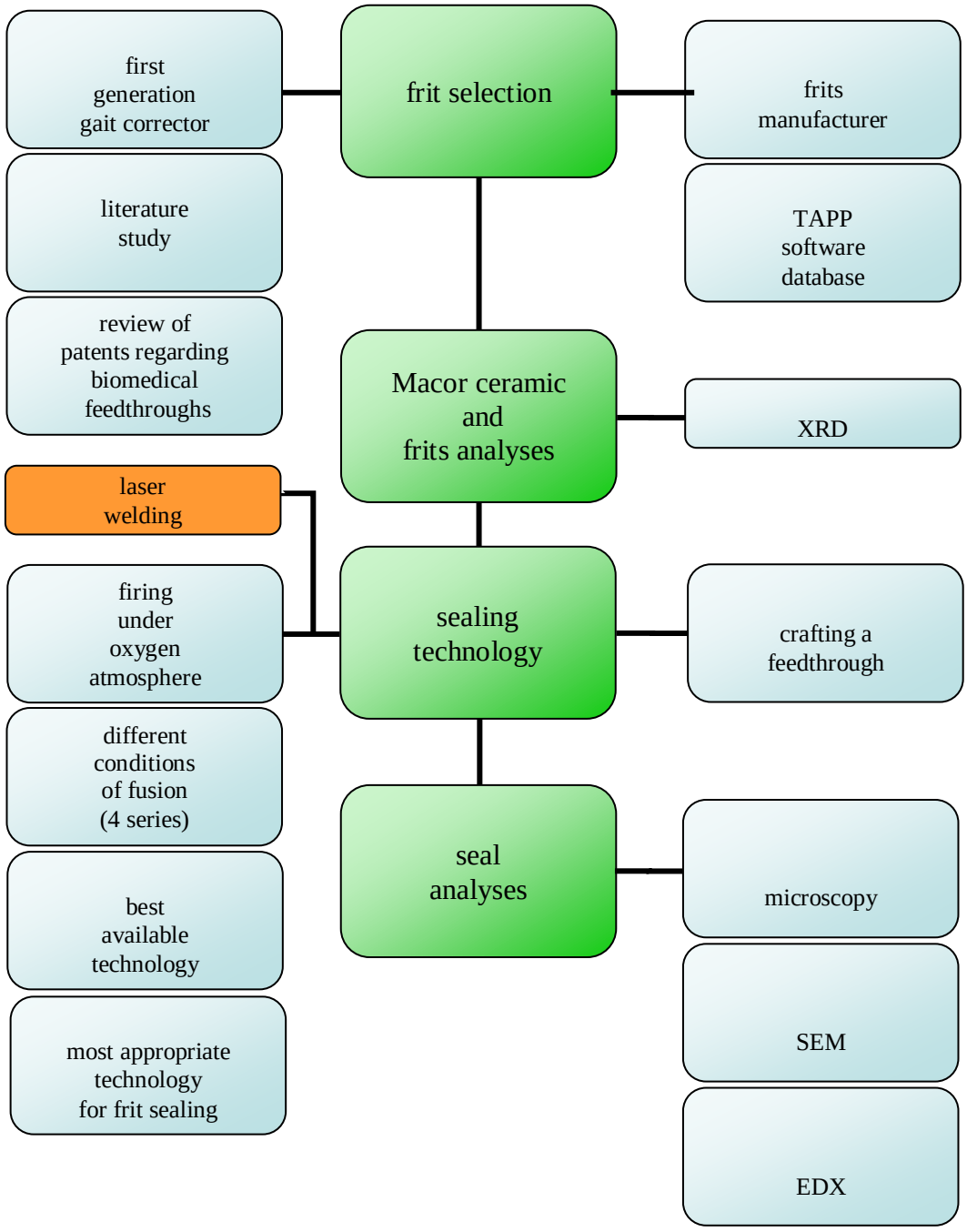


Figure 83: Organigram of feedthrough manufacturing and analysis

Within this pilot study we didn't make any fixture for holding the pins firmly in a place. The consequence was that the procedure of embedding (figures 84) was repeated several times until all frits were embedded in a suitable way.

Figures 84a: GLP and 84b: sample preparation

Silica based structures (figures 13 and 15) have primarily covalent bonds (figure 7). With lower cooling rates microstructure is crystalline. Higher cooling rates, impurities and addition of certain elements or oxides propagate formation of glassy structure [48]. While $TiO_2$ and $Al_2O_3$ are amphoteric oxides (table 4) and they can act either as network creators or destroyers, majority of oxides ($B_2O_3$, MgO, CaO, BaO, $Na_2O$) in frits act as network destroyers and consequently propagate formation of glassy microstructure (figures 15 and 16). Frits R1, R2 and R3 contains enough quantity of $SiO_2$ that microstructure is composed of minor constituents in crystalline phase (figures 30 to 34). With addition of different oxides, also nature of bonding is changed. Instead of covalent bonds, presence of mixed covalent-ionic bonds is expected within fused seals. Still, the additions of different oxides are set in a way, that melting point is not dramatically increased (figure 26). For that matter, covalent bonding is still dominant. Addition of oxides does not influence only on nature of bonding mechanism, but also on structure formation. Instead of pure tetrahedral structure we can expect partial formation of octahedral and cubic structures of oxides [48].

For prediction of the melting temperatures of the frits we used thermochemical calculation software (TAPP). Since it is earlier version, we manage to calculate only the influence of main oxides on microstructure formation (phase diagrams, free Gibbs energy) (figures 17-20). The results were used for rough estimation only.

With the XRD analysis we divide frits according to diffractograms (figures 30 to 34); our conclusion was that the frits are in glassy state with minor (or almost none) parts of the microstructure in a crystalline state.

From x-ray results (similarity) we can divide frits into three groups based on similarity of patterns:

- frit R1
- frits R2 and R3
- frits R4, R5 and R6

Further analyses partially confirmed this simplified distribution.

Major emphasis was on microstructure analysis (figures 36-60). The seal formations vary among series. Within first two series we have lower and also fine dispersed porosity due to achieved higher green density. Wetting of Macor ceramic is more problematic at lower temperatures (first series). Machine milling is reflecting in higher porosity within seal. There is no sign of fine dispersed porosity as in previous series. Consequently smaller volume of the seal is formed but at vacuum stage it is expected that this kind of porosity can be more efficiently lowered and eliminated. The wetting of Macor ceramic is not problematic. While at first two series is apparent that porosity formation is conditional to position of Pt wire, porosity in last two series is more even dispersed.

Appearing of the porosity diminish  presence and importance of the wetting angle. Hydrophilic surface (in general frits R4, R5 and R6) has low contact angle, good wettability and adhesiveness and high solid surface free energy. Results of the formed seals are more comparable within 2$^{nd}$ series. Combination of high porosity and high wetting angle negatively reflects on sealing using frits R2 (figure 39) and R3 (figure 40) at sealing temperature of 900 °C. Macor ceramic is known as non-wetting (room temperature). Since the chemical compositions of the frits are very similar to borosilicate phase in Macor and with introduction of high temperature fusion, this phenomenon can be successfully overcome. Still, as in our case, variations in chemical composition quickly reflecting on physical and chemical properties of the formed seals. Once more it was proven, that only carefully selected materials and procedures in initial state of manufacturing can provide expected results.

Frits can be defined based on microstructure analysis in the following way:

- frit R1 is not suitable for our application because of high melting temperature
- frit R2 fully seal and wet the surface within second series, porosity vary from low (1st series) to high (3rd series); wetting angle is higher than of other frits
- frit R3 completely seal the surface (except at 3rd series), last two series possess huge porosity; also as frit R2, frit R3 form higher wetting angle in contact with Macor ceramic
- frit R4 is similar to frit R3, but with minor porosity, within first two series the seal is fully formed
- frit R5 formed similar seal as frits R4 and R3; porosity is comparable to that of frit R4
- frit R6 can be compared with frit R2; based on microscopy, frit R6 is having lower surface tension resulting in better wetting of Macor ceramic

Table 11: Formation of seals according to series and frits

| | series 1 | | | series 2 | | | series 3 | | | series 4 | | |
|---|---|---|---|---|---|---|---|---|---|---|---|---|
| | seal formation | | | | | | | | | | | |
| frit | poor | partial | good | poor | partial | good | poor | partial | good | poor | partial | good |
| R1 | x | | | x | | | | | | | | |
| R2 | | x | | | | x | | x | | | x | |
| R3 | | | x | | | x | x | | | | x | |
| R4 | | | x | | | x | | x | | | x | |
| R5 | | | x | | x* | | | x | | | x | |
| R6 | | x | | | | x | x | | | x | | |

Table 11 is showing successfulness of seal fusion for each feedthrough series. The best procedure for frit sealing was that of the 2nd series. Except R1, all frits form a complete seal. The sealing of frit R5 was repeated separately (only one step to 1000 °C) and thus seal is not perfect, but it is expected that would be same as of R4-S2 since they are very similar. A slightly less perfect seal was attained when using the procedure for series 1. A complete seal was achieved by frits R4 and R5 and the porosity was more finery dispersed. The shape and size of the particles (hand grinding) also seems to be more efficient one to fill the hole during seal preparation.

The 3rd and the 4th series are containing large air inclusions. The formation of seal is not successful. Machine milling is not suitable, same as temperature program for the 3rd series in combination with machine milling. This is the opposite of what we expected as we thought that smaller particles with evenly distributed particle size would be better. However, it is expected that with introduction of vacuum cycle after each sealing cycle, the porosity can be more efficiently eliminated when machine milled frits are used. The reason for that conclusion is in porosity distribution. The main cause for porosity is in green density - with higher density we achieve less porosity. Hand grinding material is having randomly distributed particles size with polygonal shapes. As seen within microstructure analysis, seals from first two series possess fine dispersed porosity while this is not observed at later series. Thermodynamic conditions at 3rd and 4th series allowed that fine dispersed porosity was already grouped and formed large air inclusions.

The influence of isothermal steps within 3rd series cannot be fairly interpreted. Compared with the last series there is no evidence of any positive effect of that steps, rather conversely, optically determined formed seals of the last series are better.

Optical microscopy gave us information about porosity and seal formation, about wetting of the Macor ceramic and Pt wire. Obviously, emphasis was on porosity formation since the results of bonding were appropriate. Presence of porosity is affecting quality and functionality of the feedthrough in following ways:

- Surface of porous spaces can elicit inner tensions. Even without, this "weak spots" of microstructure are very susceptible to form a path for inner body liquids to penetrate to electronics within implanted unit (and back).
- Mechanical strength of the feedthrough that elicits porosity is much lower. Present tensions during usage will inevitably generate micro cracks which lead to deterioration of the microstructure. It is expected, that implant will be function as intended for at least 10 years. For that matter, homogeneity of the formed seal must be through all the time the same.

Elimination of porosity is very important task, but luckily this is far less to concern as would be in the case of poor bonding and wetting.

For SEM analysis we had chosen frit R6 from the 1st and 2nd series. The reason for that being the fact that formation of the seal was not as perfect as of frits R4 and R5.

We concluded that results of SEM analysis for those two frits would be in any case better. Within both series the wetting of the Pt wire with frit is perfect. Some imperfections are seen along border (an interphase is not formed) but they don't exceed 1 μm (figures 65 and 72). In both series the interphase between the Macor/frit is fully developed (figures 66 and 74). Differences among series are seen due to the amount of borosilicate phase (glassy phase) that contributed to interphase formation. At 1000 °C the process of fusion is more dynamic and the diffusion rates of elements are higher. As melting temperature of crystalline phase of Macor (fluorphlogopite mica) is 1350 °C it is not involved in interphase formation. Because of chemical similarities the interphase is not visually distinguishable within seal (figures 66, 67, 74 and 75). This is a sign that seal is not only mechanically strong, but more important very uniform. The main problem in feedthroughs is leaching along microstructure defects on the phase borders. In our case it seems that we have successfully overcome this problem. Since the optical delineation of Macor and frit is very clear, we decided to analyze the surface 40 μm deep of each phase (figures 77 to 83). Except for Si and Na all other elements actively participate in the fusion procedure. We see that the formed interphase is at least 0.1 mm wide with a considerable redistribution of elements from the frit and Macor.

Future work:

Next step is manufacturing of the second generation of the feedthroughs. The procedure will include laser welding.

Within the new generation of the feedthroughs the hole will have changed geometry and thus increased surface. The mechanical strength of that seal will be superior to previous one and it will make implanted device more reliable.

When the feedthrough manufacturing phase is over, biocompatibility and mechanical testing will begin, starting with current leakage tests in order to see, if the formed seals can prevent current leakage which can be responsible for ionic transfer in both directions – from body to embedded inner electronics and vice versa. We can perform current leakage test by ourselves since we are equipped with Digi-Ivy mini

potentiostat with DY2000 software (Digi-Ivy Inc., Austin, USA) and very precise measuring instrument Hewlett Packard 4140A pA meter/dc voltage source (Hewlett-Packard Company, Palo Alto, USA).

Since our work on feedthroughs sealing seems to be promising, we believe we can expand application to the field of sensors where encapsulation is also important. The knowledge we have gained and high added value of these products are a good motivation for us to develop and improve these high-tech products further.

# 6 Conclusions

Results of analyses for the pilot series of the second generation of the feedthroughs confirmed that we chosen correct technology and sealing material to achieve good bonding between Macor ceramic and Pt wire and thus reliable seal.

For the second generation we will use frit R4 (alternatively frit R5).

Technology will be adapted. Sealing procedure will be as shown in chart 5. First step will be sealing cycle (blue line) followed by vacuum cycle (red line). Those two steps will be repeated three times. After each step on one side of the seal new portion of frit will be added to compensate volume loss.

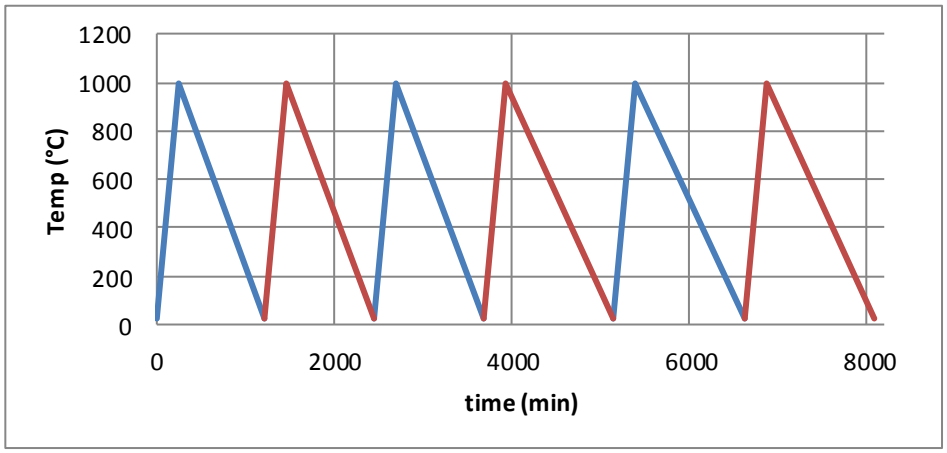


Chart 5: Sealing procedure for the second generation feedthrough

Hand grinded and machine milled frits will be used. Final selection will be upon achieved density. Optimal seal must not include any porosity.

Roughness of the surface of the Macor ceramic for this pilot study was higher than thickness of sputtered Pt and Ti. Achieved metal surfaces were not uniform. Within second generation, the thickness of the metal film will be at least 5 μm.

Coin shaped geometry turns to be successful. This geometry also facilitates easier embedding of the frits.

Appropriate fixture will be made to hold pins firmly in correct position.

At the end of procedure we will laser seal the surface of the formed seal. That way it will be established additional barrier and improved air tightness of the implanted unit.

Performed analyses confirm the formation of the seal between Macor ceramic and Pt wire. It is meaningful that biocompatibility and other testing are done only after suitable feedthrough manufacturing since functionality of the feedthrough is based on materials and microstructure constituents that were formed (and not on that, which were used since they are not necessary the same ).

# 7 Bibliography


1. Rozman, J., et al., *Implantable stimulator for selective stimulation of the common peroneal nerve - A preliminary-report.* Journal of Medical Engineering & Technology, 1994. **18**(2): p. 47-53.
2. Rozman, J., J. Krajnik, and I. Tekavčič, *Selective stimulation of the common peroneal nerve : correction of drop foot in three patients.* Eur. j. phys. med. rehabil, 1997. **7**(3): p. 75-80.
3. Rozman, J., J. Krajnik, and M. Gregorič, *Selective stimulation of the common peroneal nerve for hemiplegia: long-term clinical follow-up.* Basic appl. myol, 2004. **14**(4): p. 223-229.
4. Strojnik, P. and P.H. Peckham, *Implantable stimulators for neuromuscular control. In: Bronzino JD (ed) Medical devices and systems, The biomedical engineering handbook 3rd ed.* CRC Press, Taylor and Francis Group, Boca Raton, FL, 2000.
5. Davis, J.R., *Handbook of Materials for Medical Devices.* 2003.
6. Temenoff, J.S. and A.G. Mikos, *Biomaterials; the intersection of biology and materials science.* Pearson international edition, Pearson Prentice Hall, 2008.
7. Hench, L.L. and J. Wilson, *An Introduction to bioceramics*. 1993: World Scientific.
8. Dee, K.C., D.A. Puleo, and R. Bizios, *Biomaterials, an Introduction to tissue-biomaterial interactions.* 2003, Wiley.
9. Park, J., *Bioceramics: properties, characterizations and applications*, in *Springer Science+Business Media, LLC* 2008.
10. Nicholson, J.W., *Chemistry of Medical and Dental Materials*. 2002: The Royal Society of Chemistry, RSC Materials Monographs.
11. Callan, C., *Encyclopedia and dictionary of medicine, nursing, and allied health, 3rd edition - Miller,B, Keane,CB.* American Journal of Occupational Therapy, 1983. **37**(10): p. 707-707.
12. Ratner, B., *Biomaterials Science, 2nd Edition An Introduction to Materials in Medicine*. 2004: Elsevier.
13. Savich, V., *Criteria for selecting powder composite materials for orthopedic implants.* Powder Metallurgy and Metal Ceramics, 2009. **48**(3): p. 216-224.
14. Webster and Merriam, *Websters Ninth New Collegiate Dictionary*. 2001, An Encyclopaedia Britanica company.
15. Jiang, G. and D.D. Zhou, *Technology Advances and Challenges in Hermetic Packaging for Implantable Medical Devices, Implantable Neural Prostheses 2, Biological and Medical Physics, Biomedical Engineering.* Springer Science+Business Media, 2010: p. 27-61.
16. xklsv.org. 2012; Available from: http://www.xklsv.org/viewwiki.php?title=Biocompatibility.
17. Wang, W., et al., *Neural Interface Technology for Rehabilitation: Exploiting and Promoting Neuroplasticity.* Physical Medicine and Rehabilitation Clinics of North America, 2010. **21**(1): p. 157-178.

18. Massia, S.P., M.M. Holecko, and G.R. Ehteshami, *In vitro assessment of bioactive coatings for neural implant applications.* Journal of Biomedical Materials Research Part A, 2004. **68A**(1): p. 177-186.
19. Dee, K.C. and R. Bizios, *Mini-review: Proactive biomaterials and bone tissue engineering.* Biotechnology and Bioengineering, 1996. **50**(4): p. 438-442.
20. García, C., S. Ceré, and A. Durán, *Bioactive coatings prepared by sol–gel on stainless steel 316L.* Journal of Non-Crystalline Solids, 2004. **348**(0): p. 218-224.
21. Yarris, L. *New bioactive coatings enables metal implant to bond with bone*. Available from: http://www.lbl.gov/Science-Articles/Archive/bone-implant-coating.html.
22. Subbu, V., et al., *Bioactive Coatings for Implanted Devices*, in *Biological and Biomedical Coatings Handbook*. 2011, CRC Press. p. 471-489.
23. Puleo, D.A. and R. Bizios, *Biological interactions on materials surfaces : understanding and controlling protein, cell, and tissue responses*. 2009, Dordrecht; London: Springer.
24. Schaffer, J., *Structure-Property Relationships in Conventional and Nanocrystalline NiTi Intermetallic Alloy Wire.* Journal of Materials Engineering and Performance, 2009. **18**(5): p. 582-587.
25. Ying, J., *Nanostructured materials*. Vol. 27. 2001: Elsevier. 222.
26. Kane, M.J., et al., *BION microstimulators: A case study in the engineering of an electronic implantable medical device.* Medical Engineering & Physics, 2011. **33**(1): p. 7-16.
27. Schneider, A. and T. Stieglitz, *Implantable Flexible Electrodes for Functional Electrical Stimulation.* Medical Device Technology, 2004. **15**(1): p. 16-18.
28. Loeb, G.E., et al., *BION™ system for distributed neural prosthetic interfaces.* Medical Engineering & Physics, 2001. **23**(1): p. 9-18.
29. Kurtz, S.M., *UHMWPE Biomaterials Handbook - Ultra-High Molecular Weight Polyethylene in Total Joint Replacement and Medical Devices (2nd Edition)*, Elsevier.
30. Bellare, A. and M. Spector, *The Polyethylene History*

*Total Knee Arthroplasty*, J. Bellemans, M. Ries, and J. Victor, Editors. 2005, Springer Berlin Heidelberg. p. 45-50.
31. Spiegelberg, S., *Chapter 12 - Characterization of Physical, Chemical, and Mechanical Properties of UHMWPE*, in *The UHMWPE Handbook*. 2004, Academic Press: San Diego. p. 263-285.
32. Smith, B., et al., *Development of a Multi-Functional 22-Channel Functional Electrical Stimulator for Paraplegia*, in *Biomedical Engineering Fundamentals*. 2006, CRC Press. p. 33-1-33-11.
33. Davis, R., J. Patrick, and A. Barriskill, *Development of functional electrical stimulators utilizing cochlear implant technology.* Medical Engineering & Physics, 2001. **23**(1): p. 61-68.
34. Yoshida, K. and K. Horch, *Selective stimulation of peripheral nerve fibers using dual intrafascicular electrodes.* Biomedical Engineering, IEEE Transactions on, 1993. **40**(5): p. 492-494.

35. Weber, D.J., et al., *Functional electrical stimulation using microstimulators to correct foot drop: a case study.* Canadian Journal of Physiology and Pharmacology, 2004. **82**(8-9): p. 784-792.
36. Bhadra, N., K.L. Kilgore, and P.H. Peckham, *Implanted stimulators for restoration of function in spinal cord injury.* Medical Engineering & Physics, 2001. **23**(1): p. 19-28.
37. Narushima, T., et al., *Fatigue Properties of Stainless Steel Wire Ropes for Electrodes in Functional Electrical Stimulation Systems.* MATERIALS TRANSACTIONS, 2005. **46**(9): p. 2083-2088.
38. Mayr, W., et al., *Basic design and construction of the Vienna FES implants: existing solutions and prospects for new generations of implants.* Medical Engineering & Physics, 2001. **23**(1): p. 53-60.
39. Yonezawa, S., et al., *Fatigue Behaviors of Ultra Fine Wires of β-Type and α-Type Titanium Alloys.* MATERIALS TRANSACTIONS, 2009. **50**(7): p. 1713-1719.
40. Nagl, M. and T. Lechleitner, *Barrier coatings for medical electronic implants.* Vakuum in Forschung und Praxis, 2005. **17**(S1): p. 47-50.
41. SCT. *Solutions in Ceramic Technologies*. 2012; Available from: http://www.sct-ceramics.com/advanced-ceramics-53-En.php.
42. Jiang, G.Q., et al., *Zirconia to Ti-6Al-4V braze joint for implantable biomedical device.* Journal of Biomedical Materials Research Part B-Applied Biomaterials, 2005. **72B**(2): p. 316-321.
43. Alberox. *Technical ceramic*. 2009; Available from: http://www.alberox.com/markets/medical/.
44. Sciences, H.S.o.E.a.A. *Electronic Devices and Circuits, Engineering Sciences 154, Covalent Bonds*. 2012; Available from: http://people.seas.harvard.edu/~jones/es154/lectures/lecture_2/covalent_bond/covalent_bond.html.
45. Chemguide. *Covalent bonding - single bonds*. 2012; Available from: http://www.chemguide.co.uk/atoms/bonding/covalent.html.
46. Corporation, S.I., *Polar Bonds and Electronegativity*. 1997.
47. Chemguide. *Ionic (electrovalent) bonding*. 2012; Available from: http://www.chemguide.co.uk/atoms/bonding/ionic.html.
48. Zdovc, M., *Žlindre s povečanim deležem SiO2 za elektro pretaljevanje pod žlindro*, in *Naravoslovnotehniška fakulteta, Oddelek za materiale in metalurgijo*. 2004, University of Ljubljana. p. 60.
49. Kopeliovich, D. *Ionic and covalent bonding*. 2012; Available from: http://www.substech.com/dokuwiki/doku.php?id=ionic_and_covalent_bonding.
50. Bloomfield, L.A. *Windows and Glass*. 2001; Available from: http://www.howeverythingworks.org/supplements/windows_and_glass.pdf.
51. Rief, A., F. Kubel, and H. Hagemann, *Optical and structural properties of a Eu(II)-doped silico-aluminate with channel structure and partial site occupation.* Zeitschrift für Naturforschung 2007. **62b(12)**: p. 1535-1542.
52. Reference, A.R., ed. *Thermal Properties of Metals*. 2002, ASM International

53. Company, T.T.G., *Macor® Machninable glass ceramic*. 2011, The Technical Glass Company. p. 7.
54. Accuratus. *MACOR Machinable Glass Ceramic*. 2002; Available from: http://accuratus.com/macorfab.html.
55. Incorporated, C. *Macor*. Available from: http://www.corning.com/assets/0/965/989/1081/1397D5E7-018E-4CF4-A34C-6814B815BCAC.pdf.
56. Moğulkoç, B., *Reflow bonding of borosilicate glass tubes to silicon substrates as fluidic interconnects*. 2010, University of Twente.
57. Harper, C.A., ed. *Handbook of ceramics, Glasses, and Diamonds*. 2001, McGraw-Hill Handbooks.
58. Corporation, F.C. *Photoveel*. 2009; Available from: http://www.ft-ceramics.co.jp/eng/corporate/history/.
59. GmbH, D.D.P.S. 2011; Available from: http://www.qvf.com/en/equipment_1/borosilicate%20glass/Composition.shtml.
60. Ltd., T.T.F.M.C. *Introduction to Fluorphlogopite Mica*. Available from: http://www.tcyunmu.com/eng/enggsjj/enggsjj10.htm.
61. Rozman, J., I. Milosev, and M. Jenko, *Platinum stimulating electrodes in physiological media.* Journal of Medical Engineering & Technology, 2000. **24**(3): p. 123-128.
62. Peclin, P., M. Zdovc, and J. Rozman, *Chronic stimulation of an autonomous nerve with platinum electrodes.* Materiali in Tehnologije, 2010. **44**(1): p. 25-29.
63. Rozman, J., *Tissue response to chronic selective stimulation of the vagus nerve of a dog using multi-electrode spiral cuff.* Periodicum Biologorum, 2006. **108**(5): p. 609-617.
64. Rozman, J., Zdovc, M., *personal communication*. 2010-2011.
65. Rozman, J., B. Pihlar, and P. Strojnik, *Surface examination of electrodes of removed implants.* Scandinavian Journal of Rehabilitation Medicine, 1988: p. 99-103.
66. Rozman, J., V. Marinković, and A. Jeglič, *Platinaste stimulacijske elektrode in mikroskopska preiskava njihovih površin po odstranitvi iz tkiva: magistrska naloga*. 1988: J. Rozman.
67. Arroyave, R., *Thermodynamics and Kinetics of Ceramic/Metal Interfacial Interactions*. 2004, Massachusetts Institute of Technology.
68. Raic, K.T., et al., *Multilayered nano-foils for low-temperature metal-ceramic joining.* Metalurgija-Journal of Metallurgy, 2008. **14**(2).
69. Zivkovic, D., et al., *Application of High Temperature Lead-free Solder in Medicine.* Metalurgija-Journal of Metallurgy, 2008. **14**(4).
70. Pelletier, J.M. and M. Robin, *METAL-CERAMIC JOINING BY LASER.* Journal De Physique Iv, 1993. **3**(C7): p. 1061-1064.
71. Knechtel, R., M. Wiemer, and J. Fromel, *Wafer level encapsulation of microsystems using glass frit bonding.* Microsystem Technologies-Micro-and Nanosystems-Information Storage and Processing Systems, 2006. **12**(5): p. 468-472.

72. Arfin, S.K., *A Miniature, implantable wireless neural stimulation system*. 2006, Massachusetts Institute of Technology.
73. Dongen, M.N.v., *A versatile output stage for implantable neural stimulators*. 2009, Delft University of Technology.
74. Marshall, M.T., et al., *(2005) U.S. Patent No. US 6,903,268*: Washington DC: US.
75. Brendel, L.R., *(2006) U.S. Patent No. US2006/0028784*: Washington DC: US.
76. Xiaohai, T.H., *(2009) U.S. Patent No. US 7,498,516*: Washington DC: US.
77. Byers, C.L., et al., *(1991) U.S. Patent No. US 4,991,582*: Washington DC: US.
78. Kuzma, J., *(1991) U.S. Patent No. US 5,046,242*: Washington DC: US.
79. Bisch, M.E., S.A. Khuhro, and D. P., *(1994) U.S. Patent No. US 5,282,858*: Washington DC: US.
80. Strojnik, P., *(1997) U.S. Patent No. US 5,640,764*: Washington DC: US.
81. Schulman, J.H., *(2003) U.S. Patent No. US 6,518,808*: Washington DC: US.
82. Clasen, R., et al., *(2004) U.S. Patent No. US 6,796,143*: Washington DC: US.
83. Uhland, S.A., et al., *(2003) U.S. Patent No. US 2003/0010808*: Washington DC: US.
84. Sprain, J.W. and A.J. Angelo, *(2007) U.S. Patent No. US 2007/0239222*: Washington DC: US.
85. Frank, J., et al., *(2008) U.S. Patent No. US 2008/031726*: Washington DC: US.
86. Makowiecki, D.M. and R.M. Bionta, *(1995) U.S. Patent No. US 5,381,944*: Washington DC: US.
87. Barbee, T.W. and T. Wieihs, *(1995) U.S. Patent No. US 5,547,715*: Washington DC: US.
88. Hassler, B.A., et al., *(1998) U.S. Patent No. US 5,782,891*: Washington DC: US.
89. Margaryan, A.A., *Ligands and Modifiers in Vitreous Materials: Spectroscopy of condensed Systems*. 1999: World Scientific.
90. Okamoto, H., *Pt-Ti (Platinum-Titanium).* Journal of Phase Equilibria and Diffusion, 2009. **30**(2): p. 217-218.
91. Biolabs, P., ed. *Assessing Biocompatibility - A guide for medical device manufacturers*. rev. 2011. 27.
92. Strojnik, P., et al., *Hermetic, implantable electronic design in laboratory settings.* Medical & Biological Engineering & Computing, 1998. **19**(4): p. 398-402.